ABSTRACT

Title: Development and Characterization of High-Strain Electrodes

Remi Delille, Master of Science, 2006

Directed By: Associate Professor/Advisor, Dr. Elisabeth Smela

This thesis, composed of three journal articles, presents a compliant electrode material, based on a novel fabrication procedure. The compliant electrodes consisted of a photopatternable, urethane matrix embedded with platinum nanoparticles. The first in the series of journal articles, "Benchtop Polymer MEMS," characterized the unloaded urethane matrix's compatibility with microfabrication and patterning processes. The second, "Compliant Electrodes Based on Platinum Salt Reduction in a Urethane Matrix," presented a unique manufacturing process for compliant electrodes, which exhibited a secant modulus under 10 MPa, an electrical conductivity of 1 S/cm, and maintained electrical conductivity under mechanical strains of 30%. The third, "High-Strain, High-Conductivity Photopatternable Electrodes," explored a modification to this fabrication method that yielded a dramatic improvement in performance: an electrical conductivity of 50 S/cm, mechanical strains of 150% without loss of conductivity, robustness after thousands of strain cycles, and low hysteresis.

DEVELOPMENT AND CHARACTERIZATION OF HIGH-STRAIN ELECTRODES

BY

Remi Delille

Thesis submitted to the Faculty of the Graduate School of the
University of Maryland, College Park, in partial fulfillment
of the requirements for the degree of
Master of Science
2006

Advisory Committee:
Associate Professor Elisabeth Smela, Chair/Advisor
Associate Research Professor Henry Haslach
Associate Professor Benjamin Shapiro

Foreword

Since this thesis consists of three multi-authored journal papers, this section will highlight the individual contributions of each of the co-authors. In "Benchtop Polymer MEMS," Mario Urdaneta conducted research on photo-patterning on non-planar surfaces, photo-patterning free-standing films, swelling measurements, biocompatibility, packaging, and formation of magnetic films. Samuel Moseley was instrumental in the fabrication of microchannels and the use of the polymers as resists for etching. In addition, he contributed to the sections on micromolding and bonding, packaging, and the methods involved in using these polymers in microelectromechanical systems (MEMS). In the journal article "Compliant Electrodes Based on Platinum Salt Reduction in a Urethane Matrix," Mario Urdaneta wrote the LabView program for resistance versus strain experiments and helped acquire data from these measurements. Kuangwen Hsieh assisted with the conductivity and Young's modulus measurements. In the final journal communication, "High-Strain, High-Conductivity Photopatternable Electrodes," Mario Urdaneta helped with the acquisition of data for the resistance versus strain and lifetime measurements.

The research included in these journal articles was guided and supervised by my advisor, Associate Professor Elisabeth Smela. She took a pro-active role in the writing and editing of these manuscripts to prepare them for publication. Without her hard work and passion, these scientific works would not have been possible.

Acknowledgements

First and foremost, I would like to express gratitude to my advisor, Dr. Elisabeth Smela, for her countless hours mentoring me in everything from writing skills to proper experimental techniques. Without her, my success as a research assistant would not have been possible. I would also like to thank the other committee members, Drs. Benjamin Shapiro and Henry Haslach, for their time and effort in evaluating my Master's thesis work.

I am equally indebted to my colleagues at the University of Maryland: Mario Urdaneta, as second author on all three journal papers, for his eagerness, aptitude, and wisdom; Samuel Moseley for mentoring me upon my arrival at the university; Dr. Marc Christophersen for many helpful discussions about my work; Marc Dandin for giving me insight and knowledge about anything electrical; Xuezheng Wang for giving me the determination to seek out explanations; and last but not least, Kuangwen Hsieh and Sebastian Perez for giving me the opportunity to mentor two gifted undergraduates.

The work and data presented in this thesis would not have feasible without the gracious, technical assistance of Jonathan Hummel and Tom Loughlin in the University of Maryland Nanocenter, Dr. Ronald Couch of Professor Inderjit Chopra's group in the Rotorcraft Center, Tim Maugel in the Laboratory for Biological Ultrastructure, and Arthur von Cresce of Associate Professor Peter Kofinas' group.

Finally, I would like to extend a special thanks to Drs. Matthew Bennett, Barbar Akle, and Donald Leo of Virginia Polytechnic Institute for providing inspiration in the fabrication procedure of the compliant electrode composites described in this thesis.

Table of Contents

Chapter 1: Introduction

1 Background and Problem Statement

In this thesis, a novel, UV-patternable compliant electrode, a material that maintains electrical conductivity while being strained or stretched, was developed and characterized. Compliant electrodes are of interest for applications such as strain gauges [1], capacitance sensors [1], flexible displays [2], electrostatic discharge (ESD) protection [3], prosthetics (e.g. retinal implants) [4], conductive textiles [5] for health monitoring and diagnostics (e.g. pulse monitors), stretchable electronics [6], and high-deformation actuators [7].

A fabrication procedure for a micropatternable compliant electrode material was pursued in this work. Patternability is critical for micro- or meso-scale devices such as retinal prostheses and stretchable circuits and could potentially enable the emergence of new technologies. Compliant electrodes must also exhibit other characteristics for successful integration into the above applications. Electrical conductivity, for example, can be low ($<10^{-3}$ S/cm) for applications such as ESD protection but must be high ($>10^{1}$ S/cm) for others such as stretchable circuits. A low Young's modulus (<10 MPa) is desirable so that large deformations can be achieved at low stress. The ability to remain conductive after many strain cycles (depending on the particular application) at high strain (>10%) is an important criterion for pulse monitors and actuators. The necessity for stretchability will be further explained

using two examples of high deformation actuators: dielectric elastomer and nastic actuators.

Dielectric elastomer actuators (DEAs) are currently used in macroscale devices such as diaphragm pumps [8], walking robots [9], and acoustic actuators [10,11]. They consist of a sandwich structure in which compliant electrodes are deposited on either side of an elastomer dielectric [7], as shown in Figure 1. When a voltage is applied to the two electrodes, electrostatic forces attract the electrodes towards each other [12]. The strain in the z-direction is translated into lateral expansion of the sandwich structure in the xy-plane, a phenomenon known as Poisson's effect (see Figure 2). The electrodes for DEAs must be compliant because they are the actuating elements and must be as stretchable as the dielectric which they sandwich.

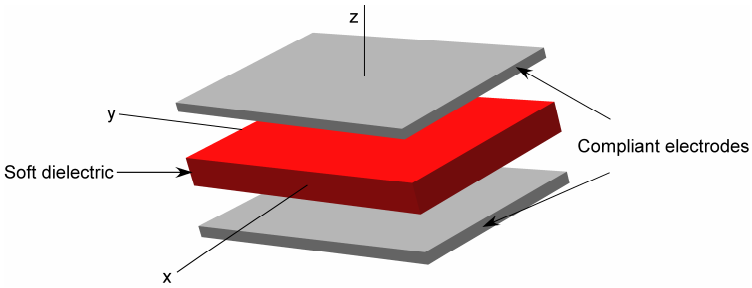

Figure 1. Components of a DEA.

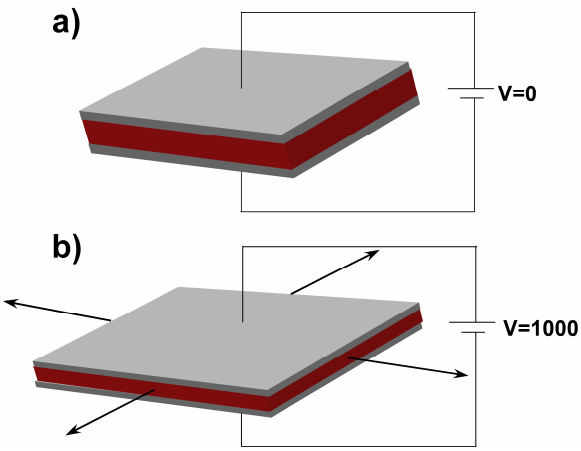

Figure 2. a) Undeformed DEA under no voltage. b) DEA displaying lateral expansion under an applied voltage.

Nastic actuators rely on electroosmotic pumping [13-15] to cause a large deformation in a compliant membrane. Figure 3 illustrates the concept of a nastic actuator. The actuator structure consists of a supply reservoir and a smaller expansion reservoir connected via an array of microchannels fabricated in an elastomer substrate. A stretchable membrane seals an electrolyte in the microchannels and reservoirs. Applying a voltage to the compliant electrodes located at each reservoir induces electroosmotic flow. The pressure required to block the fluid flow causes the portion of the membrane covering the supply reservoir to contract slightly and the portion covering the expansion chamber to bulge outwards (see Figure 3b). The electrodes for nastic actuators must be compliant because they are located in regions of the device that deform.

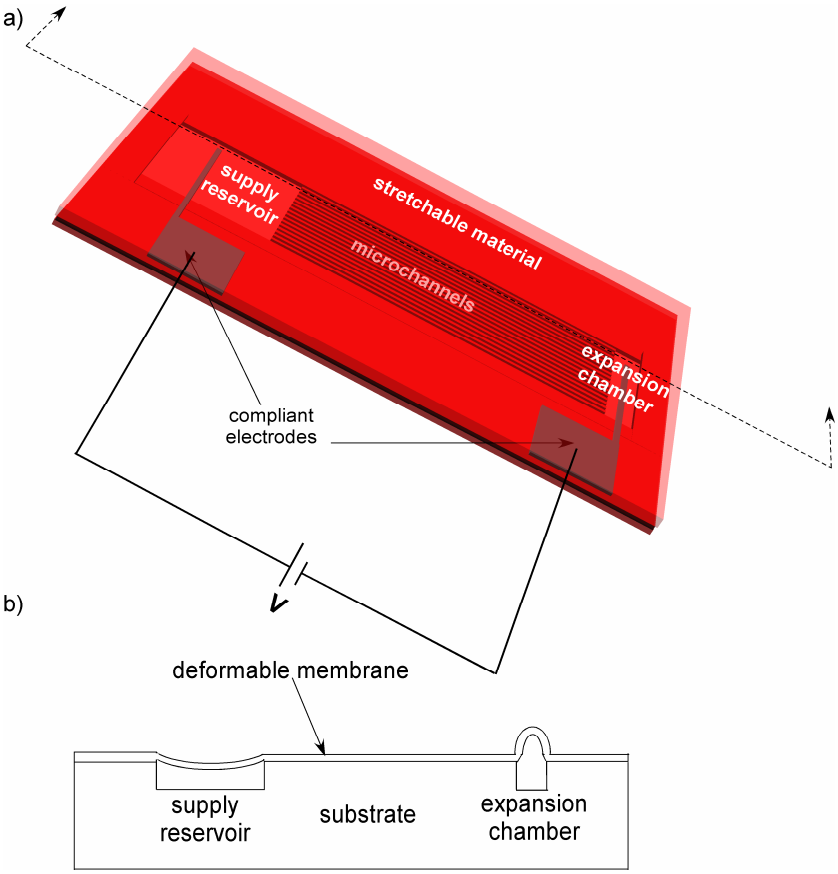

Figure 3. a) Undeformed nastic actuator. b) Cross-sectional view of a nastic actuator under applied voltage.

2 State-of-the-Art in Compliant Electrode Fabrication

Several technologies currently exist for fabricating compliant electrodes, but none completely match the requirements outlined in section 1. A common technique is depositing metal films on elastomer substrates. In one variation of this method, researchers have patterned metal films in zig-zag or sinusoidal patterns on an elastomer to produce in-plane metal patterns. Under axial strain, the patterns straighten out, thus allowing an elongation of up to 80% [16,17]. Other researchers have evaporated metal films on stretched elastomers to form out-of-plane metal

corrugations upon elastomer relaxation, allowing strains up to 100% [18]. Both of these methods are plagued by delamination at the polymer-metal interface [19,20], and stretching the elastomer during metal deposition (for out-of-plane pattern formation) is difficult to integrate into microfabrication techniques.

Researchers have used carbon grease (i.e. fluid silicone mixed with carbon particles) and graphite powder as compliant electrodes for DEAs [11,21]. These electrodes produce impressive strains (over 380%) and have an electrical conductivity on the order of 10^{-3} S/cm, but they are not a solid block or film and thus cannot be patterned using conventional microfabrication techniques.

The simplest method of producing compliant electrodes is to load conductive particles such as carbon nanotubes [1], carbon black [22], silver [23], or polyaniline [24] into an elastomer matrix. This typically results in a large rise in Young's modulus when increasing the metal content beyond the electrical percolation threshold [25]. The particles also prevent crosslinking when using a photopatternable elastomer matrix because they scatter and absorb light [23]. Table I summarizes a list of composites fabricated, and the difficulties encountered, when I attempted this technique [26].

Table I. Particle-loaded composites fabricated in Loctite 3108 (Henkel, Inc.), a photopatternable elastomer, and polydimethylsiloxane, an elastomer commonly used in microfabrication processes [26].

Binary Composite	Notes[1]	Difficulties
3108/polyaniline[2]	38 wt. %: 4.0 x 10^{-6} S/cm, 23.5 min. to cure 42 wt. %: 1.5 x 10^{-5} S/cm, 50 min. to cure	The composites were stretchable but of low electrical conductivity. Increasing the loading concentration above 42 wt. % prevented UV-curing.
3108/silver (0.5-1.0 μm dia.)	0.0 - 5.0 vol. % Ag	The silver particles prevented UV-curing of the composites at all loading concentrations.
3108/carbon nanotubes (MWNT, 60-100 nm OD)	3 vol. %: 2 x 10^{-3} S/cm, 31 min. to cure	The composites had limited strain capability (< 5 % elongation). Increasing the loading concentration above 3 vol. % prevented UV-curing.
3108/copper (3 μm dia.)	0.0 - 20.0 vol. % Cu	The copper particles prevented UV-curing of the composites at loading concentrations above 5.0 vol. %. Composites below 5.0 vol. % were neither conductive nor compliant.
PDMS/graphite[3] *(2-15 μm dia.)*	15 vol. %: 2.2 x 10^{-3} S/cm 17.5 vol. %: 3.2 x 10^{-3} S/cm 20.0 vol. %: 9 x 10^{-3} S/cm	The composites had limited strain capability (< 20 % elongation) and non-uniform electrical conductivities on individual samples.

[1] Electrical conductivities were determined using a two-point-probe.
[2] The polyaniline (PANI) was doped with 2-acrylamido-2-methyl-1-propane sulfonic acid (AMPSA) according to [27]. Loading percentages are given in terms of the PANI/AMPSA mixture.
[3] The composites were cured at room temperature for 48 hours.

One commercially-available compliant electrode material exists. Nanosonic, Inc.'s Metal Rubber is a material consisting of layers of gold nanoparticles electrostatically assembled on a polyelectrolyte [28]. It can withstand a strain of 1000% and has an electrical conductivity of 10^5 S/cm. This material, however, is prohibitively expensive and can only be purchased in large sheets [28]. It is thus unclear how to integrate this technology into microfabrication processes.

3 Thesis Outline

This thesis is divided into the following three journal papers[1]: "Benchtop polymer MEMS," [29] "Compliant electrodes based on platinum salt reduction in a urethane matrix," [30] and "High-strain, high-conductivity photopatternable electrodes" [31]. I am the first author on all three papers, and below I outline the scientific contributions of each towards the development of a patternable compliant electrode material.

In "Benchtop polymer MEMS," we characterized a family of commercially-available, photopatternable adhesives (Loctite 3108, 3340, and 3525) as MEMS materials. The elastomer 3108 (an acrylated urethane) was the material we chose as the polymer matrix for the compliant electrodes described in this thesis. "Benchtop polymer MEMS" unveiled many important features of this material that make it particularly attractive for use in patternable compliant electrodes. It showed that Loctite 3108 is photopatternable at a wavelength of 365 nm in less than one minute, thus facilitating simple patterning that is compatible with microfabrication techniques and equipment. The feature resolution was demonstrated to be as low as 35 μm using three common microfabrication methods: photolithography on a benchtop and in a cleanroom, reactive ion etching with oxygen plasma, and micro-molding with SU8 templates. In addition, deposition techniques such as spin-coating were developed, stand-alone films were patterned, and swelling and compatibility in a number of chemical solutions were examined.

---

[1] This work was also the subject of a PTC patent application, filed June 9, 2006 and entitled "Electrically conductive metal impregnated elastomer materials and methods of forming electrically conductive metal impregnated elastomer materials."

In “Compliant electrodes based on platinum salt reduction in a urethane matrix,” we developed and characterized a new compliant electrode material. The major scientific contribution of this journal article was the invention of a new compliant electrode fabrication procedure based on the manufacturing process for ionic polymer-metal composites. The fabrication consisted of mixing platinum salt into Loctite 3108 precursor, curing the mixture under ultraviolet light, and reducing the salt into platinum nodules using a reduction solution. The addition of platinum metal in the salt form into the UV-curing elastomer 3108 did not decrease the ability to crosslink the composite. The low Young’s modulus of the 3108 elastomer was preserved, even as the percolation threshold was surpassed. Initial characterization of these composites revealed a maximum electrical conductivity nearing 1 S/cm, a secant modulus under 10 MPa, and a maximum strain of about 30% before electrical failure.

In the journal communication “Photopatternable electrodes capable of 100% strain,” we presented a modification to the aforementioned fabrication method that dramatically improved the electrical and mechanical properties of the compliant electrodes. Utilizing a solvent during the reduction reaction that swelled 3108 significantly resulted in a two order of magnitude increase in the electrical conductivity (from 0.6 S/cm to 50 S/cm), a five-fold increase in maximum strain (from 30% to 150%), and a significant decrease in conductivity losses during strain cycling (from >100% to <20%).

Chapter 2: "Benchtop Polymer MEMS," *J. of Microelectromech. S.*

Remi Delille, Mario Urdaneta, *Student Member, ASME,* Samuel Moseley, *Student Member, ASME,* and Elisabeth Smela, *Member, ASME*

Department of Mechanical Engineering, University of Maryland, College Park, MD 20742

Abstract

Loctite photopatternable adhesives 3108, 3340, and 3525 are introduced for MEMS applications. These materials are patterned within minutes by exposure to UV light followed by rinsing with a solvent; no further processing is required. Because the uncured fluid is relatively insensitive to room light, this can be done on any lab bench without the requirement for a clean room. The materials can be spin-coated to obtain films, or cast between spacers for layers up to 1 cm thick, and the cured polymers range from elastomeric to rigid. These adhesives are of interest for rapid, inexpensive fabrication of relatively low-resolution features (tens to hundreds of μm) by photo-curing. They can alternatively be molded, like PDMS, to achieve high resolution, as well as irreversibly bonded after an O_2 plasma treatment. In addition, like SU8 they can be used as molds for patterning PDMS. Initial characterization of resolution, swelling, and biocompatibility were performed. One of the polymers, 3340, can be used for packaging bioMEMS-on-CMOS chips, exploiting its biocompatibility and its photo-patternability at thicknesses of 1500 μm to cover the bond wires while exposing the chip surface. As further demonstrations of the versatility of these materials, multi-level, interconnected channel structures were fabricated with a

gelatin sacrificial layer, and magnetic films were prepared, since the polymers remain patternable even with additives.

Index terms: polymer, photopatternable, negative resist, elastomer, packaging, rapid prototyping

1 Introduction

Micro-electro-mechanical systems (MEMS) began as silicon-based devices, but have since been transformed through the development of new fabrication processes based on polymers, including micromolding [32], microcontact printing [33], microfluidic tectonics [34], and decal transfer [35], to name a few. BioMEMS in particular has benefited from the innovative use of polymers [35-38], especially photocurable polymers [39-42]. These developments have been largely motivated by microfluidics [43], a field driven by the requirement for low-cost disposable devices with relatively large areas but nm to μm size features in one or two dimensions. When such devices are fabricated using classical MEMS techniques, however, the required clean-room facilities and semiconductor equipment raise the cost of manufacture. There is thus a continued interest in alternative, low-cost microfabrication methods. For example, macro-scale processes like hot embossing can be applied to polymer substrates such as compact disks for forming microfluidic channels [44]. Ink-jet printing has also been introduced to form microstructures [45,46], which has proven popular in fields such as chemical sensing. It has even been discovered that laser-printed toner can serve as an etch mask [47]. Cost and simplicity are also important for developing lab-

on-a-chip systems for medicine, yet there has been little effort in developing polymers other than PDMS [48]. Yet another motivation for such new microfabrication techniques is the possibility of using them to realize large-area, non-planar MEMS [35], which would be prohibitively expensive with conventional microfabrication techniques, as well as the possibility of ultra-rapid prototyping [49]. Finally, low-cost demonstrations of basic microfabrication concepts would benefit MEMS education if they could be performed outside a clean room.

In this paper we introduce a further development of low-cost polymer MEMS based on photopatternable adhesives that are commercially available as Loctite 3108, 3340, 3525, and related products. These materials are most appropriate for relatively large features, but with some of the techniques presented here, small features can also be realized. As we show, these materials have attractive characteristics for MEMS that are not currently available. For example, 3108 combines the photopatternability of SU8 with the mechanical flexibility of PDMS.

Loctite offers a line of photopatternable adhesives with a range of material properties; the mechanical properties, for instance, range from flexible to rigid. This paper focuses on three of these, chosen to represent the different types of polymers and to span the range of mechanical stiffness: Loctite 3108, an acrylated polyurethane adhesive, 3340, an epoxy, and 3525, a modified acrylic. Loctite 3108 is an elastomer, 3525 is stiff but flexible, and 3340 is rigid; their Young's moduli are 19 MPa, 175 MPa, and 2.5 GPa, respectively [50-52]. Selecting three polymers with a range of

stiffness allows the investigation of various applications and processing techniques. For example, the low modulus of 3108 is conducive to molding and to fabricating flexible or free-standing structures because the cured films can be easily peeled from the template and formed into different shapes. Loctite 3340, on the other hand, makes a good packaging material.

The uncured polymers are packaged ready for use and are viscous fluids with a consistency similar to honey (approximately 5 x 10^3 cP for 3108 and 3340 and 15 x 10^3 cP for 3525 [50-52]). They present no known health hazards [50-52] and can thus be used with minimum protection.

In the following Methods section, the procedures for using these polymers are detailed. The Characterization section discusses achievable linewidths, swelling behavior, and biocompatibility. The Example Applications section illustrates techniques that demonstrate the versatility of the approach.

2 Methods

2.1 Formation of a Patterned Film of Defined Thickness

All patterning steps were carried out under normal lighting conditions, which included natural light entering through two large windows and fluorescent ceiling lights. The polymers were applied onto the substrates directly from 25 ml opaque, syringe-like dispensers. To obtain defined thicknesses, the polymers were either

spin-coated or pressed between two flat surfaces separated by spacers (spacers were also used to obtain films of graded thickness).

Figure 4 shows the thickness of cured films on glass substrates as a function of spin speed, and Table 2 provides standard deviations and roughness for selected spin speeds. Thicknesses were determined with a profilometer (Dektak 3ST) or, for films thicker than 130 μm, digital calipers. Loctite 3340 and 3108 formed films of approximately equal thickness at the same spin speeds, but 3525 formed somewhat thicker films due to its higher viscosity.

Spin-coated Loctite 3525 films were smooth and uniform down to a thickness of 20 μm, which was limited by the maximum spinner speed. The other two polymers, 3108 and 3340, dewetted on glass and silicon at higher spin speeds. Neither HMDS treatment of the substrate nor dilution of the precursor in a solvent remedied this problem. These thin spun layers were also rough due to the variable consistency of the precursor fluid at that scale. As a result, the lower limit of thickness for satisfactory spun films of 3108 and 3340 is approximately 100 μm and 30 μm, respectively. Films of 3108 and 3340 thinner than 100 μm, characterized later in this paper, were fabricated using spacers instead of spin coating.

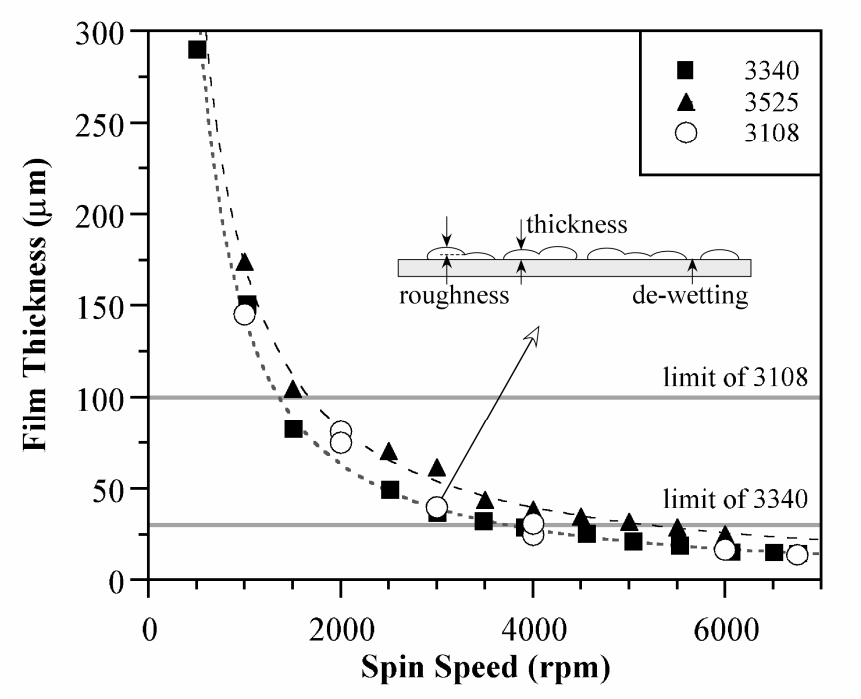

Figure 4. Average thickness of cured films as a function of spin speed. The speed was ramped up at 1000 rpm/sec, and the total spin time was 30 seconds. The dashed lines are guides for the eye for 3340 and 3525. The error bars are equal to or smaller than the size of the symbols, and thus cannot be seen in the figure. Due to roughness and dewetting, 3108 and 3340 should not be spin-coated below the indicated thicknesses. The schematic illustrates the dewetting of 3108.

Table 2. Thickness and roughness of spin-coated films.

Polymer	Avg. thickness (μm) ± standard deviation (μm) [1]		Roughness [3] (μm)		
	1000 rpm	3000 rpm	1000 rpm	3000 rpm	5000 rpm
3108	145 ± 14	42 ± 7.4 [2]	20	dewets	dewets
3340	151 ± 10	41 ± 3.7	0.06	0.09	dewets
3525	174 ± 13	62 ± 5.4	0.40	0.40	0.40

[1] Based on at least 4 samples, with 5 measurements taken on each sample at different locations.
[2] On the polymer-coated areas.
[3] Average of peak-to-peak maximum of 5 scans each 1 mm long.

Patterning was performed using both transparency masks (3000 dpi, from a commercial print shop) and higher resolution chromium-on-glass masks (USAF 1951 test masks, Edmund Optics Inc.). The polymers were cured 2 cm away from the bulb of a hand-held UV lamp (Spectroline, EN-180, center wavelength 365 nm), which delivered a power flux of 5 mW/cm^2. (Exposing the polymers to direct sunlight through a window for an hour also cured them.) The required exposure times for all three polymers are given in Table 3 for several film thicknesses. The reported curing times are those that yielded the best feature resolution (section 3.1). The curing time dependence on film thickness for 3108 was consistent with Loctite's published information for a fusion D light bulb [50]. Therefore, for thicknesses not included in Table 3, this curve can be consulted. The relationship between exposure time and thickness is approximately linear up to 1 mm; above that it is exponential. (No fusion D bulb results are given for other two polymers, and only times for thicker films are reported). Since exposure times depend on the power spectrum, they need to be calibrated for the particular type of lamp one is using. The exposure times for 3340 were significantly longer than for the other two. The numbers in Table 3 were from one batch of this polymer, but it must be noted that the times vary by up to 20% among different batches of 3340, which are produced on demand at the time of

purchase; 3108 and 3525 did not have such variations and were consistent from batch to batch. The user should therefore calibrate exposure times for each batch of 3340 before use.

Table 3. Exposure times optimized for line resolution.

Polymer	Thickness	Exposure [1]
3108	50 μm	23 seconds
	100 μm	24 seconds
	1 mm	33 seconds
3340	50 μm	4.00 minutes
	100 μm	5.75 minutes
	200 μm	6.50 minutes
3525	20 μm	20 seconds
	100 μm	46 seconds

[1] Exposures for 3108 and 3525 were tested in 1 second increments. Because of the longer exposure times required, 3340 was tested in 15 second increments. Measurements are based on at least five samples, and curing times were repeatable within 2 seconds for 3108 and 3525, and within 15 seconds for each batch of 3340. However, batch-to-batch variations in exposure time for 3340 were up to 20%.

Since these materials are adhesives, direct contact with the polymer results in bonding the mask to the substrate. To prevent this, one can use proximity lithography in an aligner. However, outside a cleanroom contact lithography is more practical, and to do this one can take advantage of the fact that the cured adhesives do not stick to all materials. Poly(dimethylsiloxane) (PDMS, Sylgard 184, Dow Corning Co.), for example, acts as a non-stick surface treatment. Wiping Sylgard 184 elastomer base (no curing agent added), onto a surface, or curing a thin layer of PDMS on a substrate, renders it non-adhesive. A mask treated with PDMS can thereby be brought into direct contact with the Loctite polymers during exposure and subsequently removed. Sylgard 184 elastomer base must be reapplied after each use, whereas a thin layer of cured PDMS will withstand 11 exposures (standard deviation of 2.3, based on five samples) before the coating delaminates and needs to be

replaced. Other examples of materials that do not adhere to Loctite include SealView (a transparent poly(olefin) wrap, Norton Performance Plastics Corp.) and Teflon. Polymer films that have been cured on non-adhesive substrates can be peeled off to form free-standing patterned films, as will be discussed in section 2.3.

Many photocurable polymers must be protected from oxygen during exposure for the crosslinking reactions to occur. Crosslinking of the three Loctites was tested in an air atmosphere to determine if protection was required for these materials. Loctite 3340 could be completely cured while uncovered in air. When the surfaces of 3108 or 3525 were exposed to air during crosslinking, on the other hand, the bulk of the polymer cured, but a layer of uncrosslinked material (approximately 30 μm and 5 μm thick, respectively) was left on the surface. This layer remained curable if the film was initially exposed for less than a minute, however, and could subsequently be cured in the absence of oxygen (this is exploited in the fabrication of microchannels, section 4.2). Loctite 3108 and 3525 were completely cured when exposed under a blanket of nitrogen or when covered by an oxygen-impermeable material such as glass or Mylar.

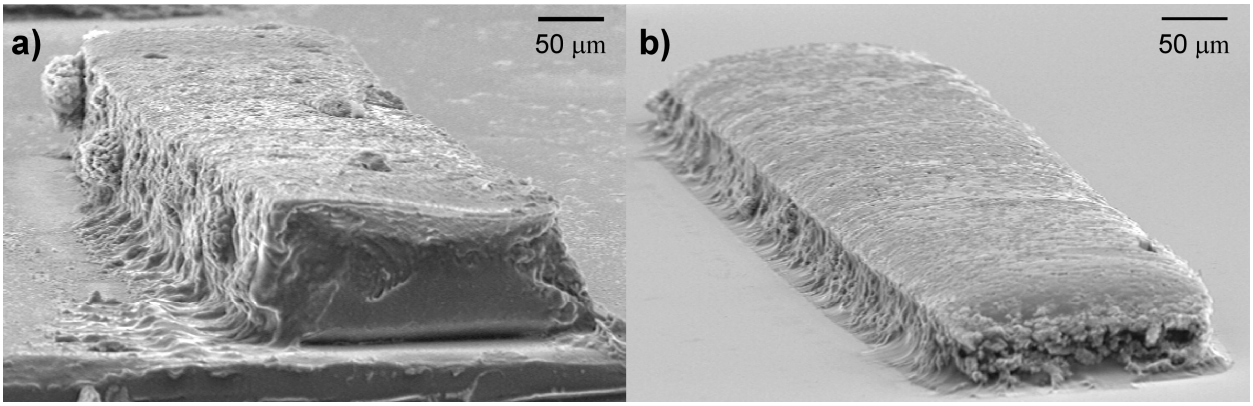

Figure 5. SEM photographs of 3108 features obtained by contact-exposure through a mask coated with Sylgard 184 elastomer base followed by developing. a) Features were developed with acetone, resulting in re-deposition of residue. b) Features were developed with ethyl acetate and water, and then sonicated in ethyl acetate for one minute, leaving cleaner surfaces. (This pattern was fabricated to be half as thick as the one in *a*.)

Uncrosslinked polymer remains liquid and can be rinsed away with a stream of an appropriate solvent, thereby developing the pattern. The best results were obtained by starting with a stream of poor* solvent, such as water, to remove uncured polymer by mechanical action, followed by rinsing with a good solvent, such as ethyl acetate or acetone. Over-exposure to a good solvent (e.g. approximately 10 minutes) led to swelling and delamination, as well as to adhesive residue redepositing on unexposed areas (Figure 5a). Redeposited residue can be removed by following a rinse in a good

* In this paper the terms "good" and "poor" are used in an informal way to express the degree of solubility relative to the other solvents used in this paper, in contrast to the formal thermodynamic definition of good ($\chi < 0.5$) and bad ($\chi > 0.5$) solvents for a solvent-polymer system.

solvent by another rinse in a poor solvent or by sonication for one minute in a good solvent (Figure 5b).

The surface morphology and sidewall profiles were highly dependent on exposure time, rinsing solvent, and post-processing (such as sonication or descum by reactive ion etching (RIE)). For example, 3340 films rinsed with ethyl acetate had smooth sidewalls that were slightly sloped in the direction of adjacent features. After RIE etching with O_2 plasma for 10 minutes, the sidewalls became nearly vertical (Figure 8b). Good line resolution in 3108 was achieved using acetone, but uncured residue re-deposited on the features (Figure 5a), while with ethyl acetate the sidewalls were clean at the expense of residue between features. In order to optimize morphology and resolution simultaneously, developing in ethyl acetate was followed by one minute of sonication in ethyl acetate (Figure 5b and Figure 8b-d). However, sonication decreased the width of the features. Therefore, additional research is needed to optimize the procedures for each of the Loctite polymers, depending on the desired outcome for a particular application.

2.2 Photo-Patterning on Non-Planar Surfaces

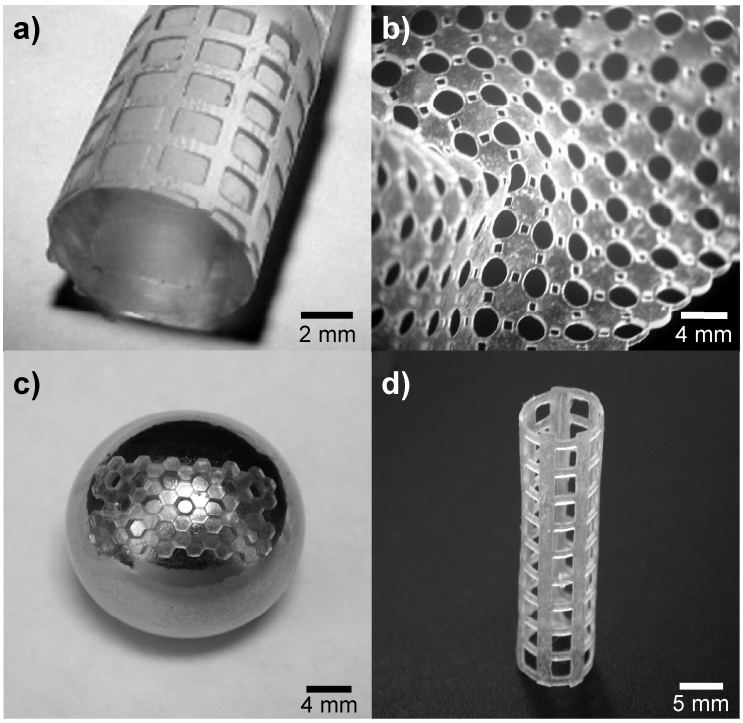

Figure 6. Patterned Loctite 3108 elastomer films. a) A grid patterned on 8 mm diameter plastic tubing; each square is 1 mm x 1.5 mm. b) Flexible, 550 μm thick free-standing film patterned on a non-stick surface and later removed, as inspired by [32]. c) Free-standing patterned film subsequently adhered onto a metal sphere. d) Free-standing version of *a*.

Because of their high viscosity, it is possible to photo-pattern the polymers on curved surfaces. Figure 6a shows 3108 patterned on the outside of a piece of plastic tubing 8 mm in diameter. This was done by wrapping a plastic mask around a 6 mm diameter cylinder and warming it with a heat gun (Wagner HT1000) to deform it into a cylindrical shape. The mask was then coated with Sylgard 184 elastomer base and wrapped around the tubing, onto which 3108 had been applied. The polymer was

exposed by rotating the tube relative to the lamp during UV exposure (45° increments, 20 sec. each). (Films of 3108 were patterned this way also on wooden pencils.)

2.3 Photo-Patterning Free-Standing Films

Loctite 3108 can be patterned and released to form flexible free-standing films (Figure 6b) similar to the structures presented by Whitesides et al. [32] Release from the substrate was achieved after exposure and development either by swelling in a good solvent or by curing the polymer on a non-stick surface.

Free-standing structures could subsequently be applied and adhered to other surfaces, flat or contoured, by applying a thin layer of uncured polymer between the new substrate and the freestanding structure and then curing a second time. Figure 6c shows a 3108 structure adhered to the surface of a metal sphere. Oxygen plasma treatment can also be used to effect adhesion (see section 2.4). These films can be stacked together and laminated, as demonstrated previously using MIMIC [32], but without the need for molds in their formation.

To produce the cylindrical structure in Figure 6d, a narrow, inflated balloon was coated with Sylgard 184 elastomer base, covered with 3108, and surrounded by a cylindrically-shaped transparency mask. After exposure and rinsing with acetone, the balloon was deflated to release the structure.

2.4 Micromolding and Bonding

PDMS is patterned by micromolding on a template [32], where the template is typically an etched Si surface or a Si substrate with SU8 features. The molding step can be followed by an oxygen plasma treatment of the PDMS and a Si, SiO_2, quartz, or glass substrate to achieve permanent bonding [53]. The same techniques can be applied to 3108 because it is elastomeric and can easily be peeled from the molding template, but fabrication is faster than with PDMS because of the photo-curing.

Molds were fabricated on silicon wafers with SU8-10 (MicroChem Corp.) exposed using the negative USAF 1951 test mask. The SU8 molds were 28 μm thick, measured by surface profilometry. The mold surface was covered with a thin layer of Teflon-containing Tri-Flow Superior Lubricant (Sherwin Williams Consumer Group) to serve as a mold release; the excess was removed with a jet of nitrogen gas. Loctite 3108 was applied to the surface, covered with a transparency sheet, and exposed using the UV lamp. To aid subsequent release, the substrate was placed in a sonication bath of methanol for 3 minutes; the film was then removed by peeling from one corner. (This step failed if the mold release compound was not properly applied.) Wiping a small amount of Sylgard 184 elastomer base on the mold, in a region away from the features of interest, created a tab that aided in removal of the cured polymer. Even the smallest features in the mold (2 μm) were transferred into the 3108 films. Micromolding resulted in higher-resolution features than photo-patterning (section 3.1 and Figure 8a) and decreased surface roughness (1.6 μm compared with 20+ μm). The surfaces of the SU8 molds had a peak-to-peak surface

roughness of only 80 nm; the greater roughness of the 3108 may have been due to poor release. Additional research is needed to develop a more satisfactory mold-release coating. One possibility is fluorocarbon coatings applied by an inductively coupled plasma (ICP); these have been used as mold-release layers for PDMS [54].

Following the same procedures as used for PDMS, 3108 can be treated with oxygen plasma to irreversibly bond it to a substrate, as well as to itself. This was accomplished by treating the 3108 and a glass substrate, or another 3108 layer, in a reactive ion etcher (120 mTorr pressure, 40 W RF power, 100 sccm O_2 flow rate, 80 sec.) and immediately bringing the surfaces into contact. The bonded pair was then placed on a hotplate at 110 ºC for 10 minutes. Attempting to remove the film resulted in cohesive mechanical failure but not debonding (the tensile strength at break of 3108 is 7.8 MPa [50-52]). This material could therefore in principle be used for decal transfer microlithography [35].

Furthermore, PDMS can be patterned by molding using any of the three Loctites as a master, in place of SU8 or Si. No mold release is needed because these materials do not adhere. This is a significant capability because PDMS is frequently used for bioMEMS, but mold fabrication has proven to be the rate-limiting step in the fabrication of devices by soft lithography [49]. Use of photopatternable Loctite for the production of masters would transfer the entire soft lithography fabrication process into ordinary laboratories, which would be particularly welcome to researchers in life sciences, and it would reduce the time required for prototyping.

3 Characterization

3.1 Feature Resolution

Because 3108 and 3340 formed poor-quality spun films, their resolution was examined in samples 100 to 200 μm thick fabricated using spacers. The resolution of 3525 was examined in thinner, spin-coated samples approximately 20 μm thick. Minimum achievable line-widths were determined using the negative USAF 1951 test mask pretreated with a layer of Sylgard 184 elastomer base. A UV light-absorbing material, such as Plexiglas or Kapton, was placed under the glass substrate to improve pattern definition by preventing light reflections. A representative result for 3108 is shown in Figure 7a.

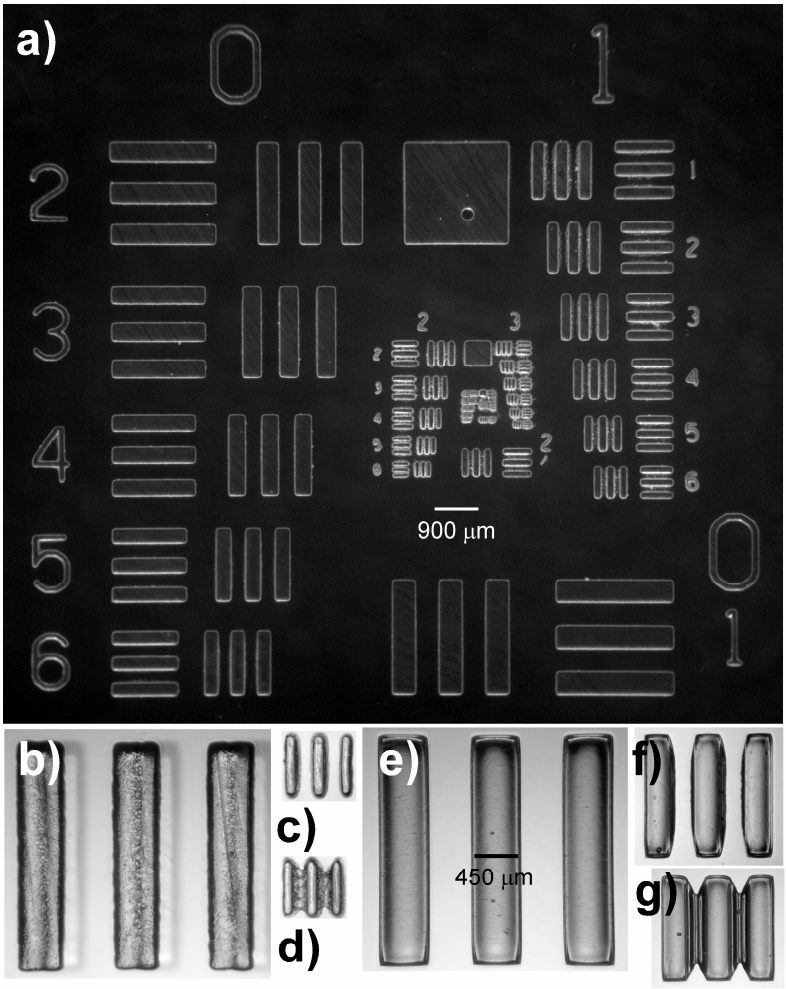

Figure 7. a) Overview of a Loctite 3108 film 110 μm thick patterned using the negative USAF 1951 test mask and developed in ethyl acetate. b-d) Representative features of a 3108 film 50 μm thick developed and sonicated in ethyl acetate, for the purpose of illustrating resolution definition. b) Bars located to the right of the 2 at the upper left of *a*). c) The smallest resolved features (125 μm width and spacing) and d) first unresolved features (110 μm). e-g) Representative 3525 features in a film 80 μm thick (*e* is in the same location as *b*). f) Smallest resolved features (250 μm) and g) first unresolved features (220 μm).

The definition of minimum achievable line-width used in this paper was the smallest feature set without residue connecting the features after developing (Figure 7c and f vs. Figure 7d and g). This is considerably more stringent than the smallest features that can be patterned, since pattern fidelity was better at the top of the film than at the base. Although not directly shown in this work, Loctite polymers should thus allow production of significantly finer ink patterns in applications such as microcontact printing than the resolutions reported here (Table 4).

Table 4. Resolution before and after a 10 minute oxygen plasma RIE descum. The polymers were developed in alternating solvent streams of ethyl acetate and isopropanol.

Polymer	Thickness	Resolution After Developing	Resolution After Descum
3108	100 μm	200 μm	140 μm
	200 μm	350 μm	250 μm
3340	100 μm	100 μm	80 μm
	200 μm	250 μm	220 μm
3525	20 μm	30 μm	---
	80 μm	250 μm	---

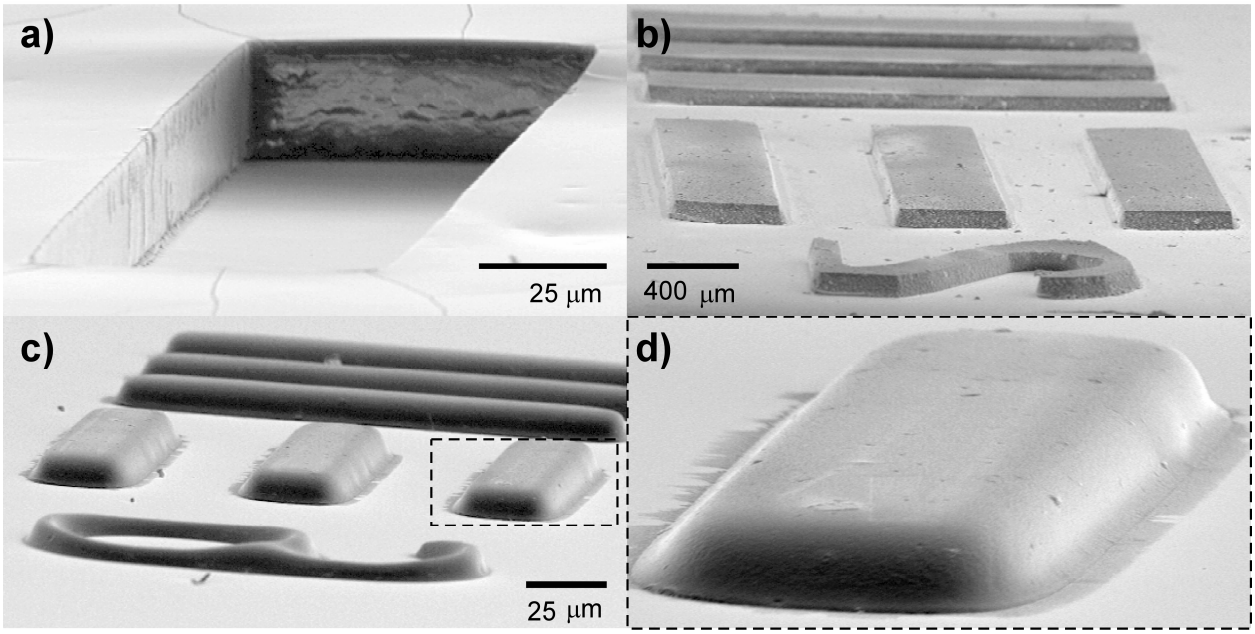

Figure 8. SEM photographs of a) a 3108 pit 28 μm deep fabricated using an SU8 mold, b) photopatterned 3340 features 80 μm thick after a ten minute RIE descum, c) photopatterned 3525 features 18 μm thick, and d) a close-up of a feature in c) as indicated by the dashed rectangle. Magnifications differ in these images.

The resolution of the polymer films depended on their thickness (Table 4). The 30 μm resolution for thin 3525 films is comparable to that previously reported for liquid phase polymerization [49]. Using a mask aligner (Karl Suss MJ-B3) instead of the UV lamp did not significantly improve the line resolution. It should also be noted that we did not systematically attempt to optimize resolution, and some improvement upon further research is to be expected.

Line resolution was examined for 3108 and 3340 films before and after an RIE descum in an oxygen plasma (120 mTorr, 150 W, 10 sccm of O_2, 10 minutes); results are shown in Table 4. The line resolution increased by as much as 30% after the descum step, which etched through the thin layer of polymer that intruded into the areas between features. RIE descum was not performed on 3525 films; however, results with 3340 suggest that RIE descum of 3525 would yield more vertical sidewalls and improved line resolution.

One of the limits on resolution is that 3108, 3340, and 3525 have low contrast in comparison with polymers such as SU8. Gray-scale lithography, which is employed with high-contrast polymers, was not successful with these Loctites, and exposure of a thick layer of uncured polymer for different times through the back of a transparent substrate did not yield cured features with different heights. Rather, exposure times that were shorter than those given in Table 3 simply led to poorer resolution or partially cured films that rinsed away during development.

3.2 Swelling

Swelling by solvents impacts the possible applications of a polymer. Understanding swelling is important because solvents are used to develop the pattern and to remove cured films from surfaces, and also as thinners and co-solvents for incorporating soluble additives. Following prior work on PDMS [55,56], we measured the swelling of the three polymers. A strip of each polymer approximately 7.5 mm x 50 mm x 1 mm (400 mg) was immersed in 14.5 ml of solvent. After 11 and 30 days, the samples

were lightly blotted with absorbent paper and weighed (Explorer, Ohaus Corp.) within 5 seconds of being removed from the solvent*. The results are summarized in Table 5 and Table 6.

Table 5. Weight increase after immersion in various solvents.

Solvent	Solvent Hildebrand Parameter [55,57] ($MPa^{0.5}$)	Weight Change (%)					
		3108		3525		3340	
		11 days	30 days	11 days	30 days	11 days	30 days
Acetone	18.6	101	101	79	80	37*	40*
Chloroform	18.8	456	460	315	311	broke apart	
Diethyl ether	29.6	24	25	34	34	5	8
Ethanol	18	69	68	80	81	27	34
Ethyl acetate	18.2	124	122	82	84	24	25
Heptane	15.1	4	4	5	6	1	4
Hexane	15.1	4	3	4	6	3	1
Isopropanol	26	48	48	66	64	14	16
Methanol	23.5	54	55	57	56	37*	33*
Methylene chloride	20.3	361	429	214	219	broke apart	
Toluene	18.2	125	123	73	74	18*	20*
Water	**47.9**	**10**	**14**	**6**	**7**	**11**	**11**
Xylene	20.2	85	86	64	67	7	6

*Cracks formed in the samples.

* The same-sample weight reproducibility was 2%. To examine the repeatability of the procedure, five different samples of 3108 were tested in acetone; these measurements agreed to within 3%.

Table 6. Weight increase after immersion in various aqueous solutions.

Aqueous Solution	Weight Change (%)					
	3108		3525		3340	
	11 days	30 days	11 days	30 days	11 days	30 days
CD30 [1] developer	18	40	34	33	12	14
Au electroplating solution (Oromerse SO Part B [3])	8	11	17	21	9	10
Ni electroplating solution [3,4]	10	9	8	10	10	11
Au etchant (type TFA [2])	71	78	35	43	14	19
Ni etchant (type TFG [2,4])	chemical reactions		20	21	20	21
Cr etchant (type TFD [2])			13	11	11	16
Al etch (type A [2,5])			chemical reactions		chemical reactions	
sulfuric acid (H_2SO_4), 95.8% [6]						
nitric acid (HNO_3), 69-71% [7]						
phosphoric acid, (H_3PO_4), 85% [7]						

Sources: [1]Shipley Co., [2]Transene Co., [3]Technic Inc.
[4] Contains small quantities of sulfuric and/or nitric acid
[5] The main ingredient is phosphoric acid, with small quantities of nitric acid and acetic acid.
[6] Caused foaming and change in solution color. [7]Turned the polymer film brown.

The solubility, or Hildebrand, parameter provides a method of predicting swelling in solvents [57]. It is generally assumed that the swelling of crosslinked polymers is greatest when the solvent and polymer solubility parameters are equal. The solvents that were used to develop the polymers after photocuring (see section 2.1) have Hildebrand parameter values δ of 18-19 $MPa^{0.5}$. Moreover, the solvents within this range of δ swelled the cured polymers the most, according to Table 5. (Plots are included in the Supplementary Materials.) For comparison, PDMS swells the most in solvents with δ from 15 to 18 $MPa^{0.5}$ [55]. Because the Hildebrand parameters favored by the Loctites and PDMS are different, one polymer could replace the other in applications for which swelling is undesirable. For example, hexane ($\delta \sim 15$ $MPa^{0.5}$) swells PDMS 30% [55], whereas it swells 3108, 3525, and 3340 under 7%. Water is the most important solvent for microfluidics and bioMEMS applications. Water swells 3108 by 14%, 3340 by 11%, and 3525 by 7%. PDMS, on the other

hand, swells less than 1% in water [55]; this value was verified using the method described above.

Swelling of the polymers was also examined in various aqueous etchants to ascertain whether they could be used as a negative photoresist for wet etching (Table 6). The results show that it withstood numerous etchants, but reacted with some acids.

Swelling in Ni electroplating solution, also of importance for MEMS, was tested as well and found to be relatively low at approximately 10% for all the polymers. Loctite 3108 can be used as a mold for Ni electroplating (see the Supplementary Materials for a figure showing features 350 μm tall). To remove the polymer, an oxygen plasma etch should be used for thick electroplated films. (Since the walls are not perfectly vertical but sloped somewhat, removing the 3108 by swelling can lift off the metal features.)

3.3 Biocompatibility

When fabricating devices for microfluidics or bioMEMS applications, the biocompatibility of materials must be considered. In our own research [58,59] we make use of bovine aortic smooth muscle cells (BAOSMC) [58], so we tested the ability of these cells to be cultured on the adhesives. Square vials of the polymers were fabricated onto cover slides. Five such slides of each polymer were attached to the bottoms of five wells of a 48-well culture flask using an adhesive known to be biocompatible (Novagard RTV-200-257). The slides were rinsed under a sterile flow

hood with ethanol, sterile water, and warm growth medium. A suspension of BAOSMC cells that had been cultured in a T-25 flask was placed into each well; the quantity of cells corresponded to 50% confluence on the surface of the slides. The 48-well culture flask was then placed into an incubator at 37 °C and 5% CO_2. Cell coverage was measured every two days for two weeks. For 3108 and 3340 samples, the growth curve showed the expected logarithmic relation with time, and the population doubled in two weeks, matching the growth pattern of BAOSMC cells in culture flasks. In the wells with 3525, cells were slower to grow on the polymer than on the surrounding glass substrate, suggesting that the material is not preferred by the cells, though not necessarily non-biocompatible.

4 Example Applications

To illustrate the versatility of the Loctite adhesives, we discuss a few examples of their use. The application for which we are now using one of these polymers is packaging lab-on-a-chip devices comprising MEMS structures and actuators built over CMOS sensors [60,61]. Other examples are given that, while not original, were made within minutes on a lab bench using inexpensive materials and equipment. The purpose of these demonstrations was not to characterize the resulting devices, but to suggest possibilities for future exploration.

4.1 Packaging BioMEMS/CMOS Chips

Packaging can be a formidable challenge in the realization of lab-on-a-chip applications. Fluids and cells may require contact with sensors and actuators on the

surface of an electrically active chip, but the bond wires must be kept dry. This is particularly difficult if the transducers are located close to the bond pads. Some researchers have glued a precision-machined well to the chip [62-64], which requires the chip to have a wide non-active perimeter [65].

We have found that Loctite 3340 works well for packaging bioMEMS/CMOS chips. In contrast, Loctite 3108 permits water and small molecules access to the bond wires, resulting in electrochemistry, as shown in the Supplementary Materials (Appendix A). Packaging was not attempted with 3525 due to a lack of clear biocompatibility. The good performance of 3340 compared with 3108 was unexpected given their similar swelling in water. Clearly, swelling is not the only critical metric for evaluating polymers for packaging.

The 3340 has significant advantages over SU8, benzocyclobutene (BCB), PDMS, and other polymers for this application. Unlike millimeter-thick SU8, this adhesive requires no mold and undergoes no appreciable shrinkage upon curing [66]. Packaging with 3340 is performed at room temperature, which was important to us because temperatures above ~120 °C damage the electroactive polymers used in our actuators. In addition, it takes only a few minutes. Films of 700 μm thickness can be readily patterned (thick enough to cover the bond wires) with tolerances of 25 μm (Figure 9a and c). Since the polymer is biocompatible and can be cured in air, it is an ideal candidate for this application.

The procedure for packaging 1.5 x 1.5 mm^2 or 3 x 3 mm^2 chips wire-bonded to a DIP40 is as follows. The DIP40 cavity is filled with 3340. A 5 x 5 mm^2 mask, consisting of a black square (either 1.2 x 1.2 mm^2 or 2.5 x 2.5 mm^2, the size of the area to be left open), is placed on the polymer directly over the chip and inside the DIP40 cavity, with one corner folded 90° out-of-plane. The mask can be manipulated by the folded corner under a microscope for alignment. After exposure (6 minutes, optimized to reduce residue) and development (alternating streams of ethyl acetate and water), which does not damage the MEMS structures, the wirebonds are completely encapsulated and thus mechanically supported. Prior to cell plating, the chip is left at ambient temperature and pressure for 24 hours to ensure that any remaining solvent has evaporated.

Encapsulation can be done using two layers of polymer (Figure 9b and d), which has a couple of advantages. For one, the 1st layer (300 μm above the chip surface) can be patterned with greater accuracy since visualization through the microscope is improved when the mask is closer to the surface. For another, the 2^{nd} layer can have a larger opening than the bottom layer so that it holds more fluid and gives easier access to the chip.

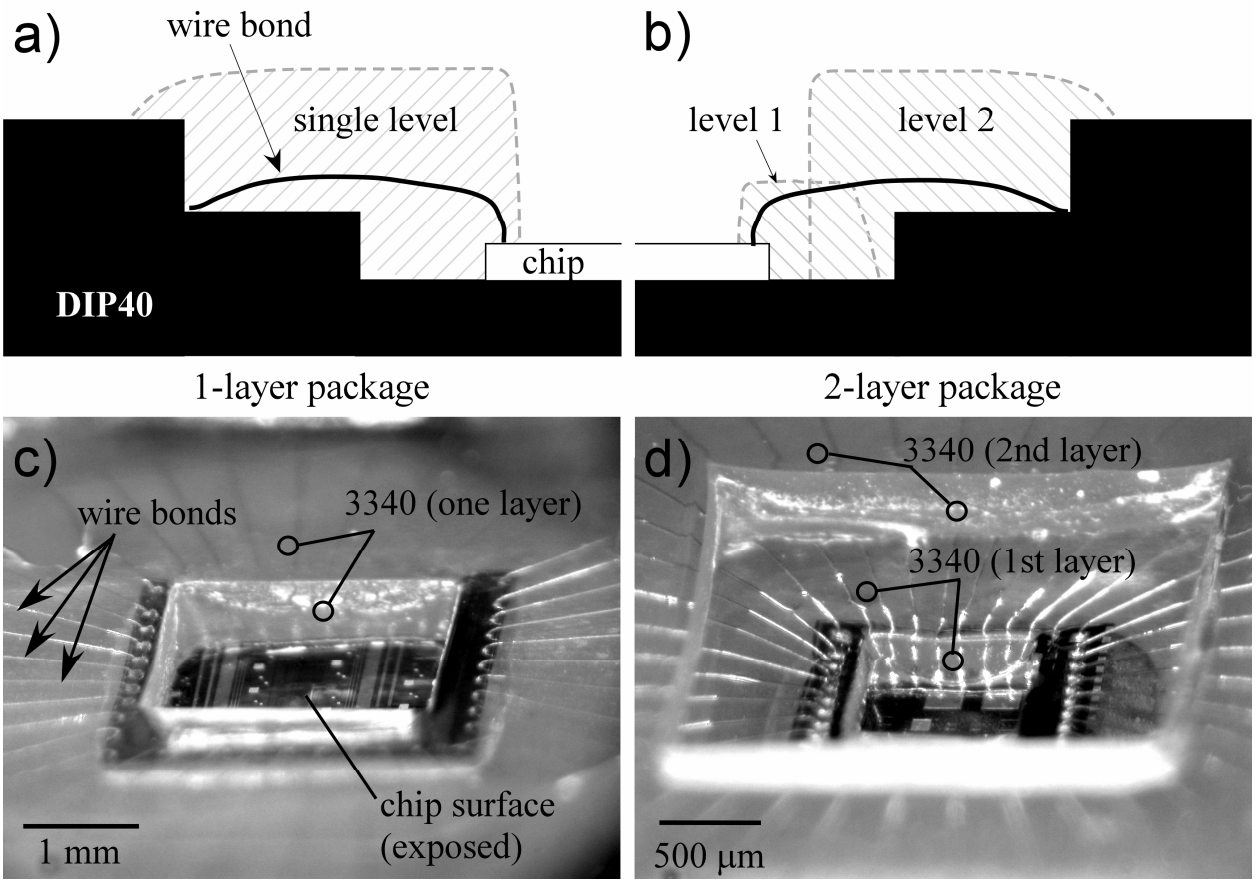

Figure 9. a,b) Schematic of the cross-section of the Loctite packaging of a chip in a DIP40. One or two layers can be used to cover the wire bonds while keeping the chip surface exposed. c) A packaged CMOS chip with overlying MEMS structures using a single layer of 3340. This layer is ~1.5 mm thick (700 μm above the chip surface). d) A two-layer packaged chip with a first layer 300 μm above the chip surface and a second that goes to 700 μm.

The accuracy achieved with this method allows packaging of the chips with more than 90% of the active chip area exposed to the cell medium and a gap of only 25 μm between the pads and the MEMS features. The main limitation of this technique lies not in the verticality of the polymer walls, but in the alignment of the mask.

Cells have been cultured inside an incubator at 37 °C and 5% CO_2 on chips with packaged CMOS capacitance sensors. Capacitance data were collected for a week without package failure. The capacitance readings were correlated with cell contact with the substrate, spreading and adhesion, and subsequent death [61]. It is important to note that exposure to ethanol (any exposure to liquid and prolonged exposure to concentrated vapor), used for sterilization in cell culture protocols, produced cracks in the 3340 and led to package failure (see the Supplementary Materials). The chips were therefore sterilized with UV light.

4.2 Microchannels

In 2000, Beebe et al. [34] presented microfluidic tectonics (μFT), a method for fabricating complete microfluidic channel systems based on liquid-phase photopolymerization of hydgrogels. In-situ creation of the channels in a packaged system offered an important advantage over prior microfluidic fabrication methods: the structures and components were fabricated simultaneously without the need for later alignment and bonding. In 2004, Harrison et al. [67] published a modification of this method based on thiolene-based optical adhesives. These channels had some advantages, including solvent-resistance and the use of a commercially available product; however, this process required a long curing time.

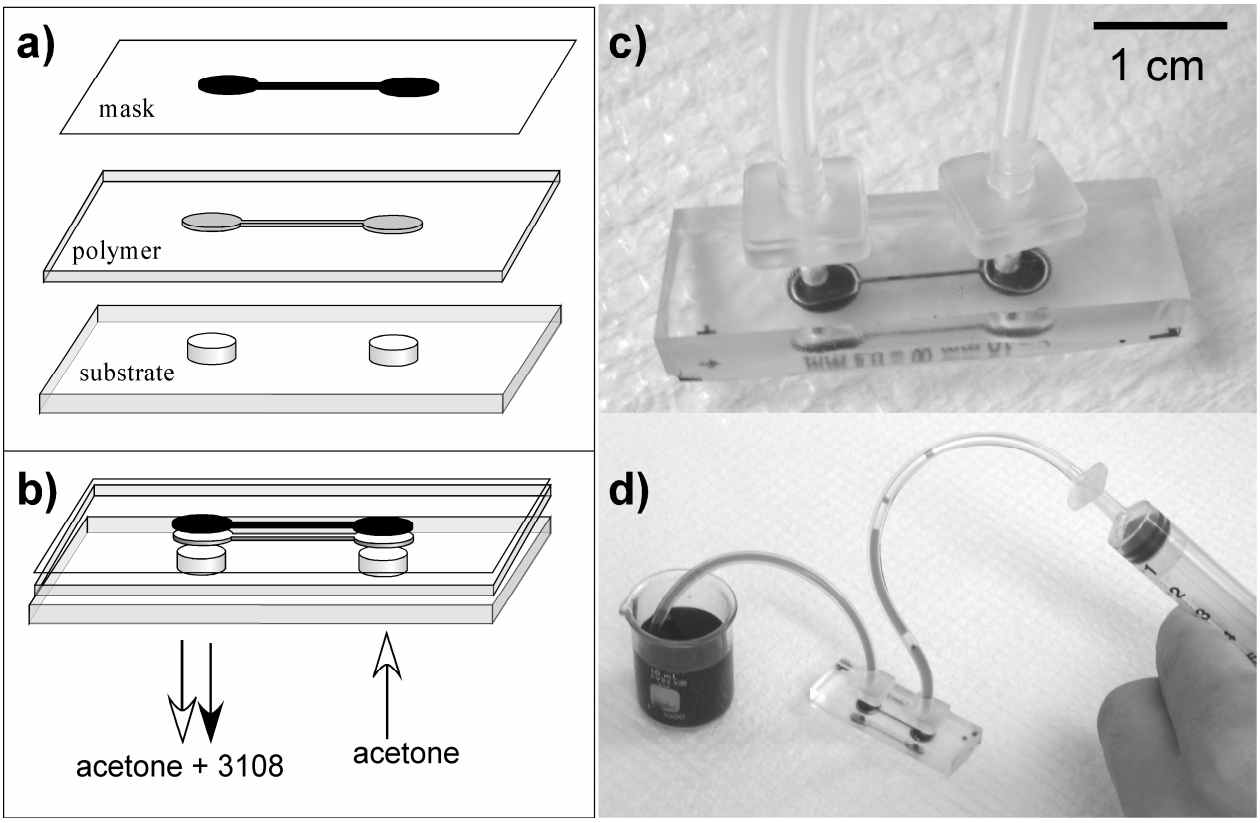

Figure 10. Microfluidic channels formed in 3108 using μFT [34]. a) The polymer is placed on a substrate with port holes, covered with a glass slide, topped with a mask, and exposed. b) The un-crosslinked polymer is flushed out of the channel using acetone. c) Completed microchannel, face-down, with a mask top cover. d) Water, dyed for better visualization, drawn through the channel after fabrication.

To fabricate microchannels, we adapted the techniques developed by these authors, as illustrated in Figure 10. A substrate was prepared by drilling holes into a glass slide (glass drill bit, 1/16" Black & Decker) or a piece of Plexiglas. The substrate was placed over a UV-absorbing material, and 3108 was dispensed onto the surface. A transparency channel mask was placed over the adhesive and aligned by eye to place

the reservoirs over the holes. A glass slide was placed over the mask to ensure flatness, and this stack was exposed to UV light. Spacers between the substrate and the mask defined the channel depth. Commercially available nylon fittings (1/16" McMaster Carr 5117k41) were pressed into the holes in the substrate, and tubes (Tygon super-soft high purity tubing, McMaster Carr 9449k11, ID 1/16") were slipped onto the connectors. A syringe (10 ml, disposable) filled with acetone was plugged into one of the hoses, while the other tube was placed into a container of acetone. The unexposed polymer was flushed out by drawing acetone from the container through the channel using the syringe to create negative pressure. The result was a sealed channel utilizing the mask as the top cover (Figure 10c). The total time to complete such a device was less than 10 minutes.

If a top cover other than the mask was desired, the mask was placed on top of that cover. For an open channel, the mask was treated with Sylgard 184 elastomer base and removed after exposure.

Certain microchannel features, such as sudden expansions and blind alleys, posed flushing problems. In this case, an open channel was first fabricated to allow complete rinsing. A cap substrate was covered with 3108 and exposed without a mask, leaving an uncured layer 30 μm thick (see section 2.1). This layer was placed, 3108-side down, onto the channel layer and exposed for an additional 30 seconds, gluing the two slides together.

4.3 Multi-Level Channels Using Gelatin Sacrificial Layers

In order to make interconnected multi-level channels, a compatible sacrificial layer is needed. Gelatin (Gelatine, Knox) is a good candidate for a low-tech, bench-top approach because it is harmless, easy to prepare, and has a melting temperature near ambient that can be controlled by the amount of water used. Open channels and reservoirs were filled with gelatin dissolved in water. Channels with a top cover were filled by injecting the mixture through the fluid ports. The channels were placed in a refrigerator and, because of the small size of the devices, the gelatin solidified within minutes, coplanar with the first channel height. A second layer of 3108 was patterned over the Loctite/gelatin base, and the sacrificial layer was removed by immersing the assembly in warm water. Multiple layers could be built up using this technique. The components of a two-layer channel fabricated with this method are illustrated in Figure 11a, and a fluid-filled two-layer channel is shown in Figure 11b. (A series of photographs showing the fabrication and testing of this device is included in the Supplementary Materials.)

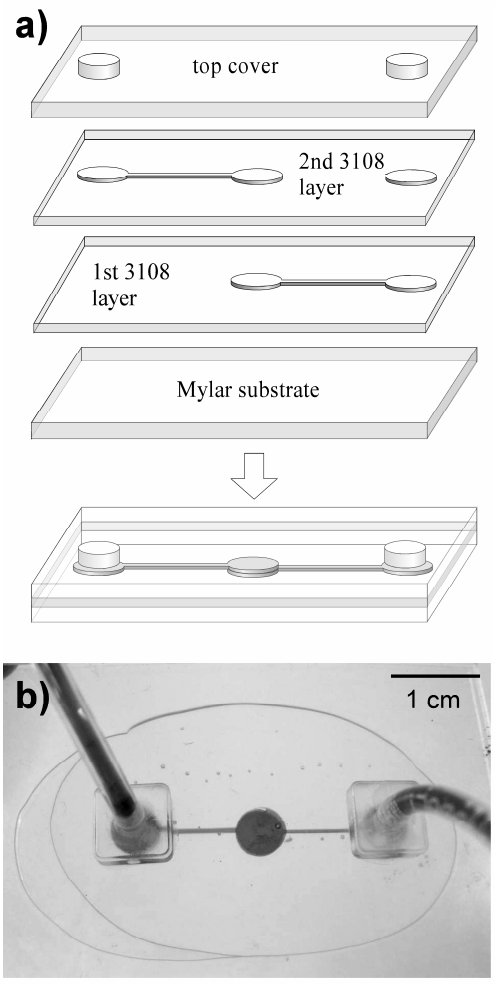

Figure 11. a) Schematic illustration of a two-level microchannel formed with a gelatin sacrificial layer. b) Water, dyed for better visualization, drawn through the channel after fabrication.

4.4 Use of Patterned Films as Resist for Etching

The polymers discussed in this paper are sufficiently impermeable to aqueous solutions (Table 6) that they could be used as a negative photoresist for wet etching. There is every reason to expect that they would also serve as effective resists for dry etching. After the exposed portions of the underlying material are etched, the

polymer is removed by immersion in a good solvent. Sonication accelerates removal. Loctite 3108 is preferred over 3340 and 3525 for this application because of its mechanical flexibility.

Use of 3108 as a wet etch mask is illustrated in Figure 12 with large features that can be readily seen in the photograph (the technique also works with small features). A Kapton film substrate was coated with a Cr adhesion layer and 1000 Å of Au by thermal evaporation. The 3108 was applied onto the Au surface, exposed to UV light for 40 seconds through a transparency mask treated with Sylgard 184 elastomer base, and developed with acetone. The Au was wet chemically etched (TFA, Transene Company Inc.), the substrate was immersed in acetone for 10 minutes, and the 3108 resist layer was peeled off.

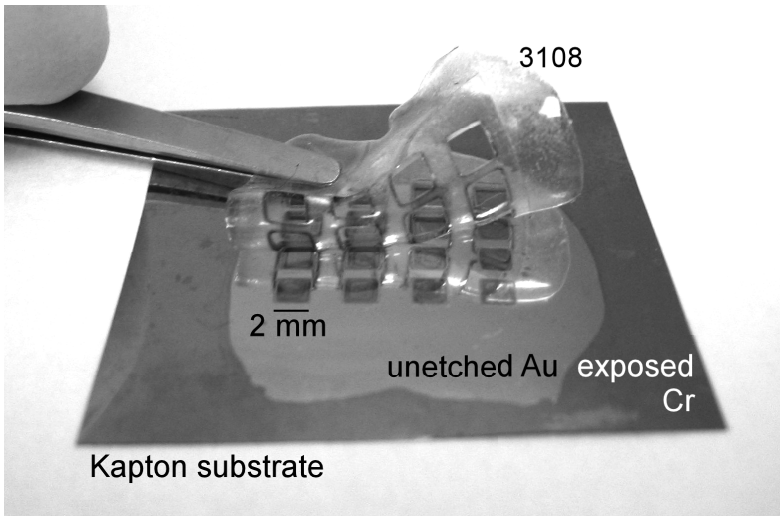

Figure 12. Use of Loctite 3108 as an etch mask. After patterning the polymer, the uncovered underlying Au was wet etched down to the Cr adhesion layer. The 250 μm thick polymer mask was then swelled in acetone and peeled off.

The Loctite polymers were particularly useful as masks for the wet etching of glass (performed in a chemical hood) with buffered oxide etchant (J. T. Baker, 7:1 with surfactant): both 3108 and 3340 allowed etching several times deeper than is usually possible with conventional photoresists. Loctite 3108 withstood 75 minutes before parts of the mask started to peel off the glass, allowing an etch depth of 40 μm. Loctite 3340 began delaminating from the glass after 48 minutes, resulting in features 27 μm deep.

4.5 Formation of Magnetic Films

One of the advantages of working with polymeric materials is that they can be readily mixed with other materials, as shown in a number of recent papers. For example, carbon [68] or silver [69] particles mixed into SU8 render it conducting, and this has been used in the formation of piezoresistors for measurement of cantilever deflection [68]. As another example, dye mixed into SU8 has been used for the formation of lasers [70]. The Loctite materials also remain patternable with additives, if they are not too absorbing or scattering, as shown by the formation of elastomeric magnetic composites using 3108 and strontium ferrite.

Magnetic materials are typically deposited by electroplating [71] or sputtering [72]. Composites [73-75] formed by mixing magnetic particles into a polymeric matrix have been screen-printed [74,76], molded [74], squeegee-coated [74], and wet etched [76]. One of the polymers that has been used as a matrix is polyimide, which can be screen printed to form 250 μm wide features or wet etched to form 200 μm features

[76]. Since polyimide is cured at 300 °C, it is incompatible with some substrates; epoxy resin (bisphenol-A-based, Shell) has also been demonstrated for 2 mm features patterned by screen-printing, and it cures at 80 °C for 2 hours [73]. PDMS has also been used to form magnetic composites [74,75], but patterning is limited to molding. It would be more convenient to use a photopatternable polymer as a host matrix. It may also be attractive in some cases, such as for the formation of compliant magnetic gaskets, for the host to be an elastomer such as Loctite 3108.

Strontium ferrite powder (HM410, particle size 1.8 - 2.3 μm, Hoosier Magnetics, Inc.) was added to 3108 and mixed with a homogenizer (T18 Ultra Turrax) until the particles were uniformly dispersed (approximately 5 minutes). The homogenizer gave visibly better particle uniformity than hand-mixing. Additives to improve particle dispersion such as those suggested in [77] were not used. The mixture was deposited and exposed in the usual ways, although light absorption by the particles increased the exposure times linearly with the volume percent of particles. Films 150 μm thick required approximate curing times of 4.5 minutes for 5% $^{V}/_{V}$ strontium ferrite (4.9 g/ml), 9 minutes for 10%, 18 minutes for 20%, and 27 minutes for 30%. Uncured material between features less than 300 μm apart was difficult to remove during development. Increasing volume fractions of strontium ferrite resulted in thicker layers of such residue. Mixtures of 20% and 30% patterned but tended to adhere to the patterning mask, even with a non-adhesive layer of Sylgard 184 elastomer base. The magnetic composites could be etched using an RIE O_2 plasma; however, the etch rate dropped with increasing volume fraction of particles: a 10%

mixture had half the etch rate of 3108 alone (0.35 μm/min at 120 mTorr, 150 W, 10 sccm of O_2, compared to 0.7 μm/min for the unloaded polymer).

A magnetically aligned film was formed by photo-curing over a magnet. The magnetic moment of samples with 10% strontium ferrite was measured as a function of magnetic field using a SQUID (MPSM-5, Quantum Design). Magnetization was calculated by dividing the magnetic moment by the sample volume (samples were 2.25 mm^2 in area and 100 μm thick).

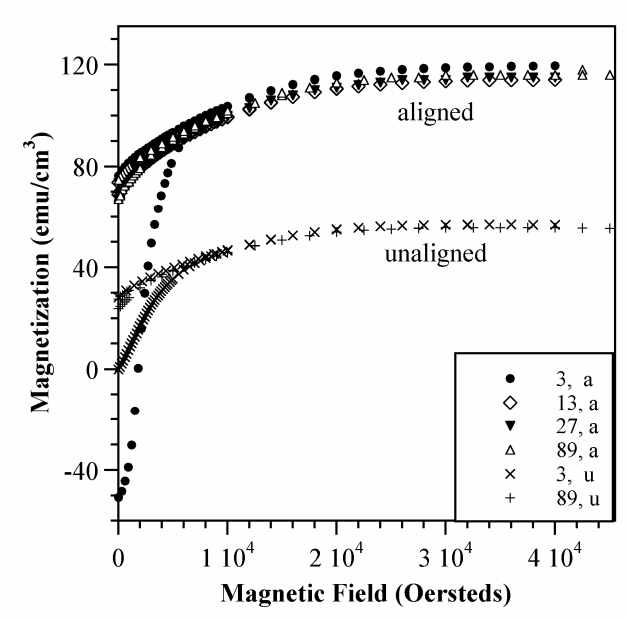

Figure 13. The magnetic saturation and remanence of 10% strontium ferrite/3108 composites. Magnetic measurements were performed 3, 13, 27, and 89 days after curing for the aligned composite sample (indicated by a in the legend), and 3 and 89 days after curing for the unaligned composite sample (indicated by u).

Figure 13 shows curves for aligned and unaligned composite samples. The aligned composite had a remanent magnetization (-50 emu/cm^3) at the start of the measurement, thus indicating that either the particles, their magnetic moment, or both, had been aligned by the field during curing, whereas the unaligned composite had no net magnetization. The aligned sample exhibited greater saturation (117 emu/cm^3) than the unaligned sample (56 emu/cm^3) (saturation obtained using the $1/H^2$ method [78]) and greater remanence after saturation (74 vs. 28 emu/cm^3). The magnetization did not decrease with time for either the aligned or unaligned samples; variations in Figure 13 were within experimental error. The magnetic properties were thus improved by aligning the magnetic particles in the composite during curing, and the effect was semi-permanent over the studied time period of three months.

5 Conclusions

We have presented a bench-top microfabrication methodology that utilizes low-cost, commercially available, photocurable adhesives. We have also performed initial characterization and demonstrated their utility as promising new MEMS materials through several examples of their use, so that others who may find these capabilities of interest can further explore their potential applications.

There are several notable contributions that these Loctite materials, and potentially also other photopatternable adhesives (such as the Norland family of UV optical adhesives [79]), can make to MEMS. The wide variety of formulations considerably extends the range of material properties available for structures and devices, as well

as the upper limit of film thickness (up to an unprecedented 1 cm). Patterning is fast compared with SU8 since no baking steps are required. Furthermore, patterning is possible on non-planar surfaces and on non-traditional materials. All three polymers can be used to fabricate templates for molding mesoscale features in PDMS with simple equipment and fast turn-around time. The fact that the materials are good adhesives for a wide variety of materials can be exploited, for example, in the fabrication of microchannels. Yet the adhesivity can also be easily prevented by coating the surface with PDMS or other surface modifications. By patterning the non-stick areas over the substrate, the principle of differential adhesion [80] could be applied in device fabrication.

Two of these polymers have features that are of particular interest. The 3108 shares some of the attractive capabilities of PDMS, including its elastomeric properties, the formation of irreversible bonds to Si and glass by oxygen plasma treatment, and biocompatibility with cells. However, the fact that 3108 is also photopatternable decreases the turn-around time for prototyping compared with PDMS. Likewise, the 3340 shares many of the attractive characteristics of SU8, but even thicker films can be produced, and a wide range of thicknesses (30 μm to 1000 μm) is achievable with a single formulation and at substantially lower cost. The 3340 has proven useful for packaging bioMEMS/CMOS chips because it is biocompatible and prevents electrolyte from reaching the bond wires.

The ability to work with all of these materials under room light and at room temperature allows photolithographic techniques to be employed virtually anywhere, and thus to be exploited by a wider community. It also opens the way for educational institutions that do not have microfabrication facilities, such as community colleges and even high schools, to demonstrate MEMS fabrication techniques and devices.

6 Acknowledgments

At the University of Maryland, we would like to thank Joshua Higgins at the Center for Superconductivity Research for performing the magnetic properties measurements, Nicole Nelson and Pamela Abshire in Electrical and Computer Engineering for performing the biocompatibility experiments, Tim Maugel at the Laboratory for Biological Ultrastructure for operating the SEM, and Marc Christophersen for examining the effect of ethanol on 3340 packages. This work was funded by the National Science Foundation under PECASE grant ECS0238861 and by the Army Research Office under MURI award W911NF-04-1-0176.

Chapter 3: "Compliant Electrodes Based on Platinum Salt Reduction in a Urethane Matrix," *Smart Mater. Struct.*

Remi Delille, Mario Urdaneta, Kuangwen Hsieh, Elisabeth Smela

Mechanical Engineering Department, University of Maryland, College Park, MD 20742

Abstract

An elastomeric but electrically conducting material is presented that is fabricated using a method inspired by ionic polymer-metal composites. The secant modulus is only 10 MPa, and yet the conductivity is nearly 1 S/cm and the material remains electrically conductive under uniaxial strains of 30%. Furthermore, this electrode material is photo-patternable. Fabrication begins with mixing the platinum salt tetraammineplatinum(II) chloride into a UV-curable acrylated urethane elastomer precursor (Loctite 3108). The mixture is crosslinked under UV light in less than a minute and can therefore be patterned if it is exposed through a mask. The salt is then chemically reduced with sodium borohydride, which results in the formation of 100 nm sized platinum nodules on the surface of the film.

1 Introduction

Materials that are electrically conductive but mechanically compliant are needed in a wide range of applications, from artificial tactile skins [81] (for e.g. robotics and prosthetics) to smart textiles [5] and artificial muscles [82]. The electrical conductivities that are required range from low (10^{-10} to 10^{-7} S/cm) for applications

such as discharge protection [3], to medium (10^{-3} to 10^{1} S/cm) for strain gauges [83] and for electrodes used in dielectric elastomer actuators (DEAs) [84,85] and capacitive sensors [1], to high (>10^{1} S/cm) for electrical interconnects and stretchable electronics [86] with low power consumption, low resistive heating, and fast response times.

The goal of this research was to produce a robust, elastomeric, high conductivity material that could be patterned using standard microfabrication methods. These compliant electrodes were expected to survive handling and use in actual applications without damage. For use in devices such as DEAs and smart textiles, the electrodes must be able to stretch tens of percent or more, without breaking or losing conductivity, and return to their original length when the stresses are removed. High conductivity was a goal because if it could be achieved, then it would be straightforward to dial the conductivity down as needed. For any microscale component or device, or any that interface between the meso- and micro-scales, including many of the applications given above, micro-patternability of the electrodes is required. The most preferable is if the material can be photopatterned, because this is a one-step, low-cost method that can be performed on large, nonplanar surfaces, as well as small, flat ones, and it thus provides flexibility in the manufacturing process and for system integration. In addition, the research aimed to produce a material that could sustain high strain rates without damage.

Compliant electrodes are already available, but none display all of the characteristics previously described. Thus, the development of a novel material could extend the capabilities of existing devices as well as enable new technologies. There are four existing types of compliant electrodes: conducting-particle-loaded polymers, thin metal films on polymer substrates, carbon grease or graphite powder, and electrostatically assembled materials. Loading metallic particles into a polymer is simple and common, but while particle-loaded elastomers can reach reasonable conductivities, the Young's modulus climbs orders of magnitude with loading, so the materials are no longer elastomeric [25,26]. While photopatterning is possible using this approach, the particles (metals, carbon black or carbon nanotubes, even inherently conducting polymers) strongly interfere with the process due to light absorption or scattering [23,26]. High strains and conductivities can be obtained by coating elastomers with thin metal films [20], and the achievable strain can reach 50-100% if the film is corrugated out of plane (e.g. by stretching the substrate during deposition [18,85,86]) or if it is sinusoidally-shaped in the plane [16,17], but this approach suffers from delamination at the polymer-metal interface, especially at defects [19,20]. Although metal films on elastomer substrates have been patterned using microfabrication methods such as lift-off [6], patterning can be challenging, particularly in cases where the photolithography steps cause elastomer swelling or adverse chemical reactions, and pre-stretching is incompatible with microfabrication. Carbon grease [8,21,84] and graphite powder [10,11,87] are currently used in dielectric elastomer actuators and allow impressive areal strains of more than 300%. Unfortunately, they can rub or wear off, and they cannot be integrated into

microfabricated devices. Layer-by-layer electrostatic self-assembly incorporating metal nanoparticles produces excellent robustness, elasticity (hundreds of percent strain), and conductivity [28], but the resulting materials are very expensive, and methods for integration with microfabrication techniques are unclear (they are produced in the form of free-standing sheets).

This paper introduces a new fabrication method to form robust, conductive, photopatternable elastomers. The approach was inspired by the electrode formation process used in ionic polymer-metal composites (IPMCs) [88-91].

2 Experimental

2.1 Fabrication of Composite Films

Films were fabricated using the elastomer Loctite 3108 (Henkel), the metal salt tetraammineplatinum(II) chloride (Sigma-Aldrich), and the reducing agent sodium borohydride (Sigma-Aldrich). Loctite 3108 is an acrylated urethane with a proprietary structure. The fabrication procedure consisted of three steps: mixing the salt into the elastomer precursor, exposing the mixture to ultraviolet light to form the elastomer and pattern the electrode shape, and chemically reducing the salt to metal in the borohydride solution.

The tetraammineplatinum(II) chloride (2.74 g/cm^3) was ground with a mortar and pestle for 5 minutes. It was added into the 3108 elastomer precursor (1.08 g/cm^3

[29]) in concentrations varying from 0 to 15 vol.% and hand-mixed for 20 minutes, followed by homogenization at 10,000 rpm for 2 minutes (T18 Ultra Turrax homogenizer). Air bubbles in the mixture were removed in a benchtop vacuum chamber (10 Torr, 5 hours).

Loctite 3108 is an adhesive, but it does not stick to SealView, a transparent polyolefin film (Norton Performance Plastics). The 3108/salt mixture was sandwiched between glass slides protected with SealView. Spacers were used to define a film thickness between 100 and 150 μm [29]. The front and back sides of the film were exposed to a dose of 100 mJ/cm^2 of UV light (Spectroline EN-180, center wavelength 365 nm, power flux of 5 mW/cm^2 [29], 20 seconds on each side). The film was peeled from the SealView and cut into rectangular samples (25 mm x 15 mm x 150 μm for conductivity measurements and 35 mm x 3 mm x 100 μm for Young's modulus and resistance versus strain measurements).

To chemically reduce the platinum salt, the films were immersed in an aqueous 30 mM solution of sodium borohydride (Sigma-Aldrich) at 60 °C for 5 hours. The reduction step was repeated one time.

2.2 Conductivity Measurement

Conductivity was measured using the four-point-probe technique [92] with four 0.64 mm diameter wires spaced 2.75 mm apart. A digital multimeter (Fluke 8505A) supplied the current to the outer pair of electrodes and also measured the voltage drop

across the two inner electrodes. The geometric correction factor G for thin rectangular samples was used to determine the resistivity ρ:

$$(1) \qquad \rho = G \times R = \frac{\pi}{\ln(2)} \times \mathrm{t} \times \mathrm{R}_1\left(\frac{\mathrm{b}}{\mathrm{s}}, \frac{\mathrm{a}}{\mathrm{b}}\right) \times R$$

where t is the film thickness, a the film width, b the film length, s the probe spacing, and R the resistance [93]. The function R_1 is tabulated for various geometries in [93].[2] This is a conservative estimate because the electrical conductivity was tabulated using the thickness of the entire film, as opposed to the thickness of just the metallized surface layer.

2.3 Secant Modulus Measurement

The secant modulus was measured using a force-strain transducer (Model 300B, Aurora Scientific) [94] as an approximation to the Young's modulus. Custom LabView software controlled the arm on the transducer head to provide a strain rate of 0.67%/sec, and it also monitored the force. The secant modulus was obtained from the slope in the region from 0.5-2.0% elongation on the stress-strain curve.

Figure 14 displays the experimental test set-up. Since the composite films are soft, the sample was rigidly clamped at both ends to avoid tearing. Two aluminum blocks served as a clamp at one end, and two 3 mm x 5 mm transparency strips glued to both lateral faces of the film served as the other clamp. Loctite 4304 was used to adhere

[2] With the correction factor, the calculated electrical resistivity was 25% higher than that calculated from $\rho = RA/l$, where A and l are the cross-sectional area and length of the sample, respectively.

the transparency clamps to the composite samples. The use of 4304 minimized slip since it is 100 times stiffer, at a reported Young's modulus of 1.6 GPa [95], than 3108. A 500 μm diameter through-hole was drilled in the center of the transparency clamp, and 0.002" diameter wire (California Fine Wire Company) was passed through the hole and tied to the arm of the tensile tester.

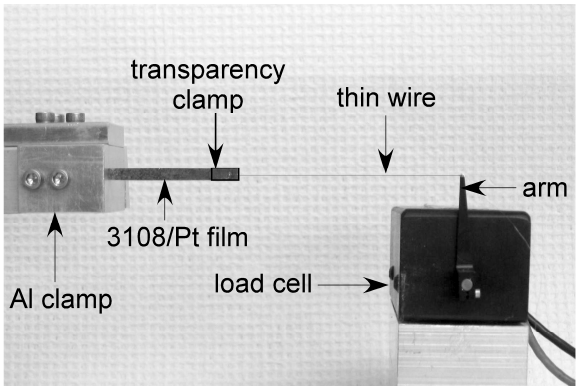

Figure 14. Set-up for secant modulus measurement.

2.4 Scanning Electron Microscopy

Scanning electron micrographs were taken with an AMRAY 1820D at 20 kV. Energy dispersive (x-ray) spectrometry (EDS) was also performed on a 12 vol.% 3108/Pt sample with an EDAX DX-4 x-ray microanalysis system. Samples were cryogenically freeze-fractured to obtain cross-sectional images.

2.5 Resistance vs. Strain Measurements

For resistance versus strain measurements, the samples were mounted in an Instron 8841 tensile tester (2 kN Dynacell load cell) with aluminum clamps. They were

elongated at 0.2%/second. The resistance was measured using a two-point-probe technique in which a voltage supply (Lambda LPD-422A-FM) applied 5.04 volts across a 10 kΩ resistor in series with the 3108 composite film. A 1.48 MΩ resistor was used when the resistance of the sample surpassed 40 kΩ. During uniaxial loading, a LabView data acquisition program monitored the voltage drop across the sample. The 2 kN load cell had +/- 0.25% repeatability for a force range of 20-2000 kN. Due to the size and softness of the composites, the force on the composite samples was always less than 2 N. The resolution was thus unknown in this range, and force data could not be extracted from these measurements for monitoring the stress during strain cycling.

3 Results and Discussion

3.1 Composite Formation

The salt had a large distribution in the sizes of the crystallites, from below 1 μm to a maximum of ~100 μm. The crystals did not dissolve appreciably when mixed into the Loctite 3108, or during curing.

The exposure time needed to crosslink the 3108 was determined in a previous work [29] and was unaffected by salt loading. This is in contrast to conducting nanoparticles, which absorb or scatter light, as mentioned above. This route to the formation of conductive elastomers is therefore unique in completely preserving

photopatternability, and relies on the fact that the metal salt is transparent, unlike the metal.

Upon reduction, the material became gray, opaque, and shiny [26]. Some of the platinum precipitated in the reduction solution and not in or on the polymer, seen as an increasing gray cloudiness of the solution over time. The amount of reduced platinum in the composites is thus unknown.

The metal formed primarily on the surface, as shown in Figure 15. The SEM images show that the platinum (bright regions) precipitated into nodules approximately 100 nanometers in diameter on the elastomer surface (dark). Energy dispersive spectroscopy (EDS) confirmed that these nodules were Pt. EDS detected no Cl or N anywhere in the composite, showing that all the ions had left the polymer.

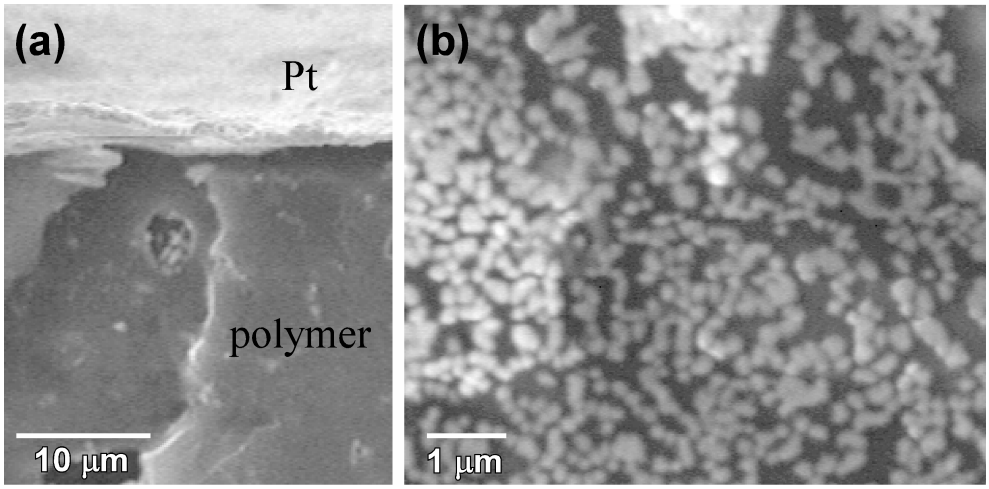

Figure 15. (a) Cross-sectional view of a sample loaded with 11 vol.% salt prior to reduction. (b) Overhead view of the surface of a sample loaded with 7 vol.% salt prior to reduction.

The adhesion of the metal to the elastomer was tested using a standard tape test (Scotch Magic, 3M). This is a threshold test: it determines whether the metal adheres more strongly to the elastomer or to the tape. Since the composites were more elastic than the tape, application of the tape test resulted in a strain of ~80% when the tape was peeled off, which added further stress. Only dustings of metal were removed by the tape, even when the test was applied multiple times to the same sample. The amount of dust that came off increased with the salt loading, but the metal adhered better to the sample in all cases (i.e. the appearance of the composites did not change following the tests).

Water swells Loctite 3108 by 10% [29], but the fact that the Pt was only on the surface, and that there were no ions left in the polymer, suggests that the sodium

borohydride did not appreciably penetrate into the polymer, and that the reaction occurred when the salt diffused to the polymer surface. The nodules indicate a nucleation process. This implies that the ionic species have a quite small partition coefficient (the ratio of the concentration of salt in the polymer to that in the water at equilibrium), which is not unexpected for charged species in a hydrophobic matrix.

3.2 Conductivity vs. Salt Loading

When a host matrix is loaded with a conducting material, the conductivity typically increases sharply at the percolation threshold, the loading at which the particles become sufficiently interconnected to provide electrical conduits across the material [22,25,69,96]. To map the conductivity vs. loading curve for the 3108/Pt composites, samples were prepared with salt concentrations from 0 to 15 vol.%. It is important to note that the results are presented with respect to salt loading concentration, which does not represent the amount of conducting platinum in the composite.

As illustrated in Figure 16, below 5 vol.% (region I), the conductivity of the composites was too small to register on the multi-meter, which had an upper limit of $2.65 \times 10^{8}\ \Omega$ ($>4 \times 10^{-6}$ S/cm). The conductivity became measurable at a salt concentration of 5 vol.%, and in region II, the percolation regime, increased approximately one order of magnitude with each additional 1 vol.% (from 10^{-4} to 0.5 S/cm). Based on percolation theory, the relationship between concentration and conductivity should follow a power law. The solid line in Figure 16 is a power law fit

to the data within the percolation regime. Above 10 vol.%, the electrical conductivity remained constant.

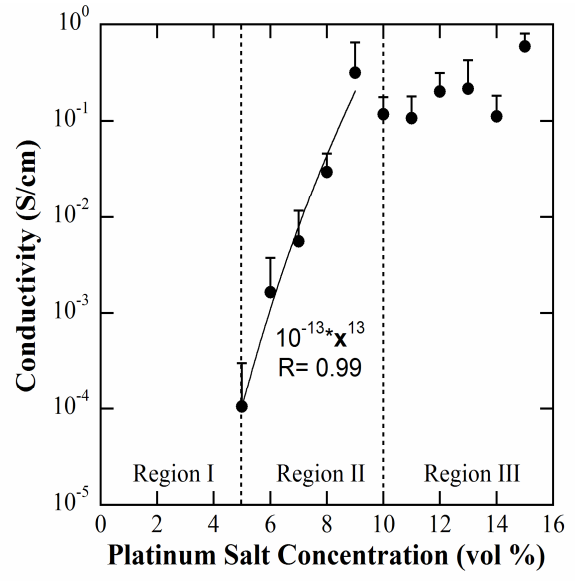

Figure 16. Percolation curve for the 3108/Pt films (semi-logarithmic scale). The error bars show the standard deviations, based on three measurements each on at least four samples (negative error bars not shown), and the line is a power law fit.

Interpreting the data based on percolation theory, platinum particles produced by the reduction process should be sufficiently isolated from each other in region I that they do not form long conducting paths across the sample [25]. Figure 17a shows the surface of a sample at 5 vol.%, the point at which electrical conduction just became measurable. Some particle interconnection is visible, consistent with the electrical measurements. The distribution of platinum on these samples is strikingly similar to that reported by Nemat-Nasser et. al. for Flemion-based IPMCs [91].

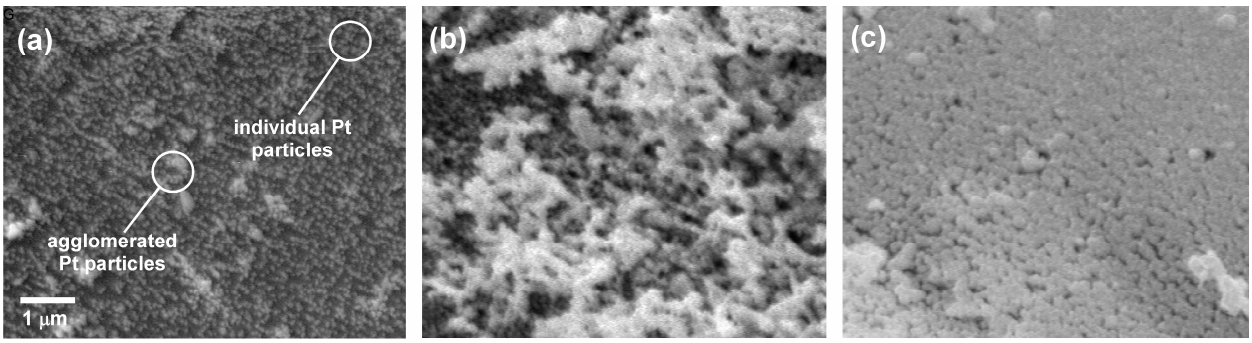

Figure 17. Scanning electron micrographs of 3108/Pt composite surfaces with (a) 5 vol.% (b) 10 vol.%, and (c) 15 vol.% platinum salt loading at 15 kV. (All micrographs are at the same magnification.)

Figure 17b shows the surface of a 10 vol.% sample, at the upper end of the percolation regime, on which large spanning clusters are visible and individual platinum nodules are difficult to discern. The large error bars in Figure 16 reflect the inhomogeneous distribution of metal. At a loading of 15 vol.%, Figure 17c, the Pt homogenously covered the entire surface, consistent with the data in Figure 16 showing that these samples have the highest conductivity and smallest variation between samples.

The variations in conductivity are not critical for technologies that operate at high voltage and low current, such as DEAs, but for other applications this may be unacceptable. Techniques have been developed for IPMCs to increase platinum homogeneity, such as introducing dispersing agents during the reduction process [89,90], and these may be applicable to the 3108/Pt composites. Another technique

used in IPMCs is electroplating a layer of gold or platinum to enhance interconnection between the particles [89,90,97]. This was done on a 12 vol.% 3108/Pt sample, giving an increase in conductivity from 0.2 to 12 S/cm, but a 40% drop in maximum strain before electrical failure. This method is therefore inappropriate for elastomeric conductors. Varying parameters during the manufacturing procedure, such as temperature [89], solution concentration [89,98], immersion time [98], or homogenization conditions [96] has been shown to improve the spatial distribution of the metal in polymer-metal composites. More specifically, increasing the mixing time and temperature improved homogeneity in carbon black [96] and polyaniline [24] loaded composites.

3.3 Secant Modulus

The key goal of this research was to produce a conductive material that remained elastomeric. The secant modulus at each loading was therefore measured. The stress-strain curve for a 14 vol.% composite is shown in Figure 18a. The slope of the curve changed over the strain range, as is typical of most polymers [99]. We arbitrarily chose 0.5-2.0% strain as the interval from which to estimate the moduli, and these are plotted in Figure 18b. Each point represents the average of 10 measurements each on at least four samples. One standard deviation error bars, not shown, are approximately the same sizes as the symbols in the figure.

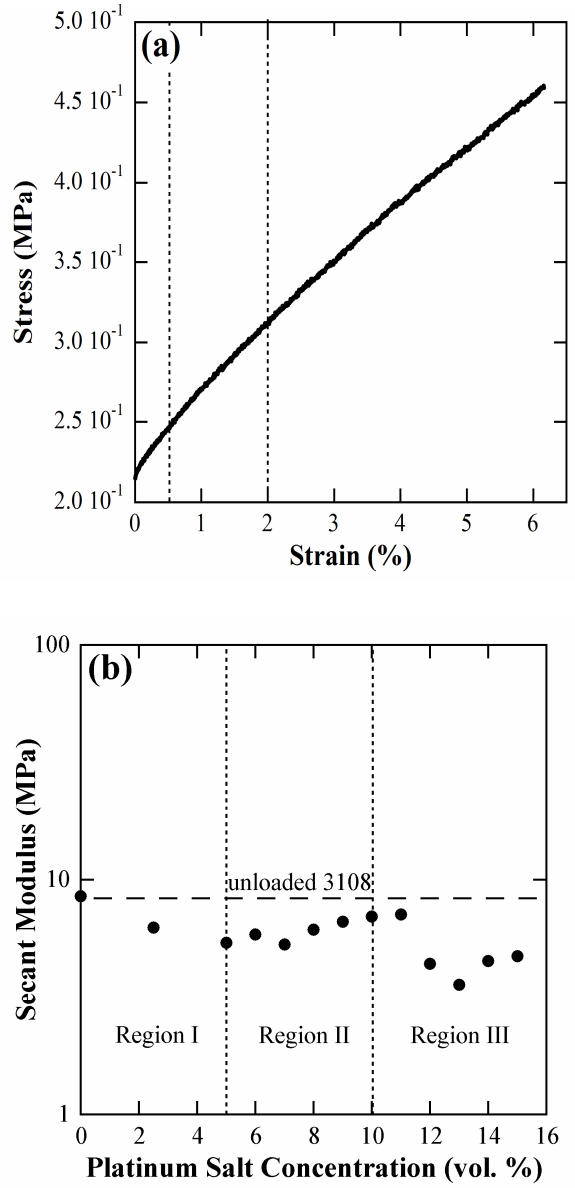

Figure 18. (a) Stress-strain curve for a 14 vol.% 3108/Pt sample. The secant modulus was obtained from the slope between 0.5 and 2.0% strain. (b) Secant modulus with respect to platinum salt loading (semi-logarithmic scale).

The modulus of unloaded 3108 was 9 MPa. As the platinum salt concentration increased, the modulus, surprisingly, decreased. The interaction between the

platinum particles and matrix is not a mechanically-reinforcing one, as observed in most particle-loaded composites [99].

Voids are known to decrease the modulus [99]. Small platinum salt crystals were present in the mixture prior to UV exposure, and the polymer must form around them. We hypothesize that nano- to micro-scale voids were thereby produced during the reduction step when the salt diffused out of the polymer. These small voids would be difficult to observe in SEM images of sample cross-sections. In the more highly loaded samples, tens of μm-size macro-voids were observed (Figure 19), which may account for the large drop in modulus in region III (10-15% loading).

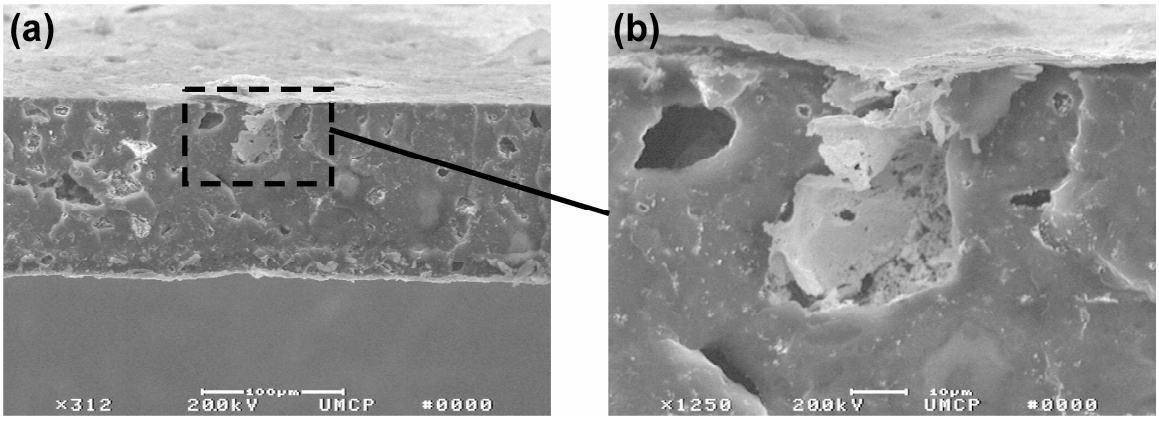

Figure 19. (a) Micrograph of cross-section of a 3108/Pt composite film formed with 11 vol.% salt concentration. (b) Close-up shows a macro-void filled with Pt and two smaller macro-voids.

3.4 Resistance under Uniaxial Strain

Compliant electrodes must remain conductive under strain, and preferably experience minimal electrical and mechanical hysteresis. The resistance under uniaxial strain was measured for samples above the percolation threshold (14 vol.%). Since viscoelastic effects are minimized at low strain rates [100], the samples were elongated at 0.2%/second.

Figure 20a shows the resistance of a sample cycled ten times from 0 to 5% strain followed by 10 cycles from 0 to 7.5% (not shown) and 0 to 10%. The resistance was approximately linear with strain. It increased irreversibly during the first cycle to 5% (from 4.6 to a maximum of 16 kΩ), and again during the first cycle to 10% (from 9.8 to a maximum of 250 kΩ), marking a significant electrical hysteresis or unrecoverable electrical conductivity due to the Mullins effect [92]. During subsequent cycles, the maximum resistance dropped somewhat, stabilizing at 13 kΩ for the 5% strain cycles (Figure 20b). Following the ten cycles to 5 and 10%, the electrical resistance in the relaxed state recovered to 8.7 and 23.5 kΩ, for a net resistance increase of 89% and 140%, respectively.

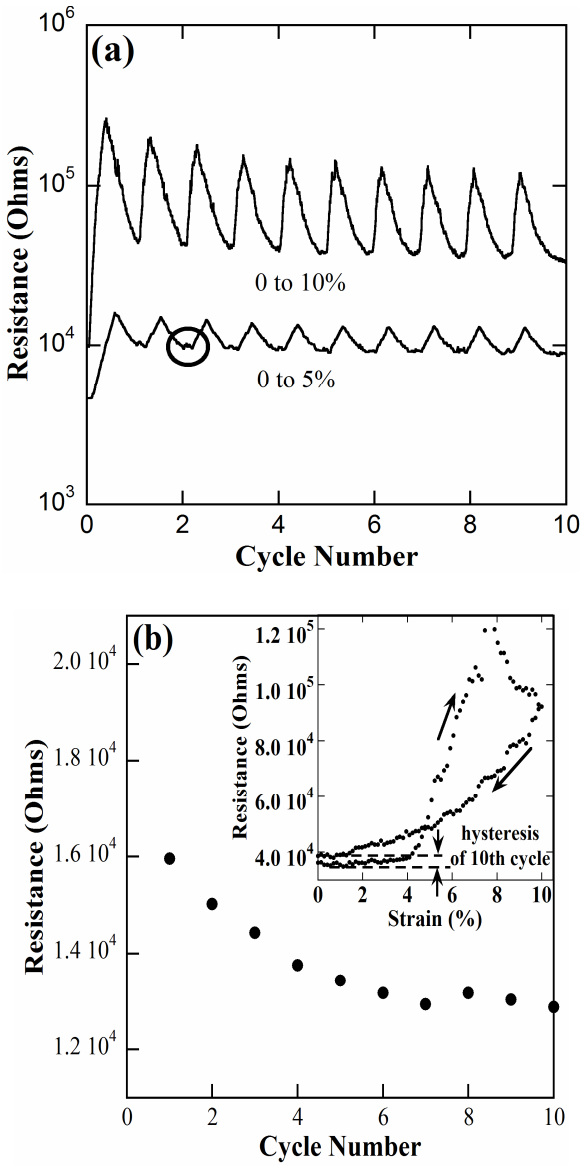

Figure 20. (a) Resistance of a 14 vol.% 3108/Pt composite during strain cycling from 0 to 5 and 0 to 10% elongation (semi-logarithmic scale). (b) Maximum resistance during strain cycling to 5%, where the inset is a resistance-strain hysteresis loop for the tenth cycle from 0 to 10% strain.

During relaxation from 5% back to 0% elongation, the arms of the tensile tester moved together faster than the film contracted, marked by the circled region in Figure

20a, so that the films buckled. This mechanical hysteresis was less pronounced during the subsequent cycles to 10% elongation. Slow relaxation has been observed in other particle-loaded composites and was attributed to stress softening [92].

The samples were also strained to electrical failure (Figure 21). The resistance increased approximately exponentially with strain up to 26.5% (the average of three samples, standard deviation of 5.4%), at which point it suddenly jumped beyond the detection limit of the experimental set-up; this was defined as electrical failure. (This is not the same as the ultimate strain, which is the point at which the material ruptured mechanically.) The samples recovered their conductivity when the strain was reduced. Applying the percolation model, electrical failure occurred when the platinum nodules become sufficiently separated so as to break all electrical paths across the sample.

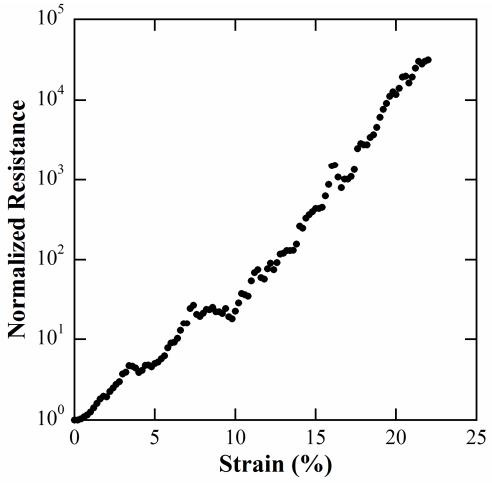

Figure 21. Strain to electrical failure at a strain rate of 0.2 %/second for a 14 vol.% composite. The normalized resistance is R/R_0, where R is the resistance at the specific strain value and R_0 is the initial resistance.

Since this material is being explored as a compliant electrode for applications such as dielectric elastomers, it is necessary to know its mechanical integrity under high strain rates. Composite samples at 5, 9, and 13 vol.% loading were cycled 10 times each at a strain rate of 6.7 %/second to 13% strain and then examined using SEM. In the 5 and 9 vol.% samples, the high strain rates created micro-cracks (< 1 μm in width and 5 μm in length), a phenomenon also observed on the surfaces of IPMC transducers [90]. In the 13 vol.% sample, the platinum wrinkled (Figure 22). The images suggest that either the platinum may not be not strongly bound to the polymer and partially delaminated from it, or that the composite plastically deformed and formed wrinkles upon relaxation. Given that cracks and wrinkles do not interfere with electrode performance in IPMCs and thin metal films on elastomers, they are unlikely to interfere with the conductivity or modulus of these composites, but this requires further study.

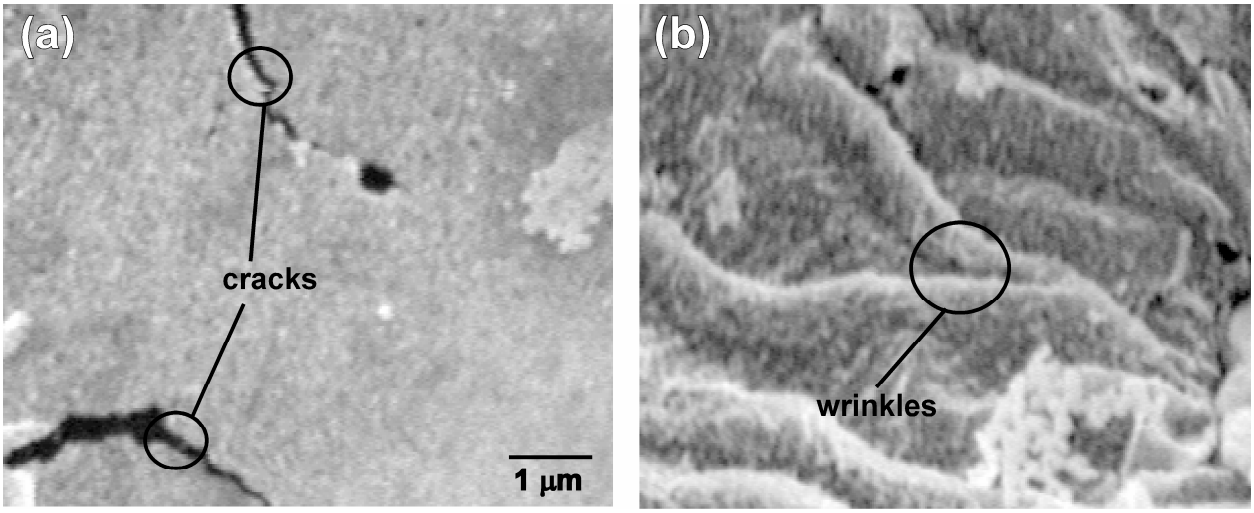

Figure 22. SEM micrograph of sample surfaces exhibiting (a) micro-cracks and (b) wrinkles after 10 cycles at high strain rate (6.7 %/sec). (Magnification is the same in these images.)

4 Conclusions

A novel compliant electrode fabrication method has been presented that offers several advantages over existing methods. The fact that the metal is initially put into the material as a transparent salt allows the elastomer to be photo-cured, which means that the electrodes can readily be patterned into any desired shape and integrated with microfabricated components. The formation of a metal skin on the surface of the polymer that is made up of small nodules keeps the modulus of the composite low. Since the metal is formed as it emerges from the polymer during the reduction process, it adheres well, and the material can thus readily withstand strains of tens of percent without significant loss in performance. The conductivity, after an initial "break-in", is not lost with strain cycling at low strain rates, although this must still be shown at higher strain rates.

The Pt-coated elastomers, while promising, are not yet ideal, however: maximum strains and strain rates, hysteresis and mechanical lag, and cost should all be improved. The fabrication method has not been optimized in any way, and there is every reason to expect that there can be significant improvements in performance by adjusting the numerous process parameters. Furthermore, the use of other metal salts, such as silver nitrate or copper sulfate, could substantially reduce the cost.

The performance of these conductive elastomers is already sufficient for low and medium conductivity applications. The composites in region I have a conductivity below 10^{-4} S/cm, but the upper end of this region is useful for low-current applications, for which conductivities as low as 10^{-10} S/cm are acceptable. In addition, for films in regions II and III, the conductivity, and the essentially linear change in conductivity, make these materials of use as strain gauges. The goals set out at the beginning of the paper were therefore substantially met. However, the performance is not yet sufficient for the highest conductivity applications or for dielectric elastomer actuators. The modulus is acceptable, but additional research is required to produce materials that can undergo hundreds of percent strain at extremely high strain rates for millions of cycles.

5 Acknowledgements

We would like to thank Dr. Donald Leo of the Virginia Polytechnic Institute and his graduate students Barbar Akle and Matthew Bennett for guidance in the IPMC

fabrication technology. All SEM photographs were taken at the Laboratory for Biology Ultrastructure at the University of Maryland under the helpful supervision of Tim Maugel. The strain versus conductivity measurements would not have been possible without the gracious assistance of Ron Couch and Dr. Inder Chopra. Last, but not least, we are grateful to Samuel Moseley for machining the aluminum clamps and translational stage. This research was supported by the Army Research Office through the MAV MURI Program (Grant No. ARMY-W911NF0410176) with Technical Monitor Dr. Gary Anderson.

Chapter 4: "High-Strain, High-Conductivity Photopatternable Electrodes," *Adv. Mater.*

Remi Delille, Mario Urdaneta, and Elisabeth Smela
Mechanical Engineering Department, University of Maryland, College Park, MD 20742

Electrically conductive materials capable of bending and stretching are useful for a wide range of applications such as smart clothing [5], flexible interconnects and displays [2,101], strain gauges [1], implants (e.g. retinal prostheses) [4], and dielectric elastomer actuators (DEAs) [84], to name a few. The necessary mechanical extensibility varies from minimal (< 5% elongation) for applications such as retinal implants that only require conformal contact to a surface [4], to small (10-20%) for DEAs used in devices such as loudspeakers [11], to medium (20-60%) for conductive textiles used for health monitoring and diagnostics (e.g. pulse or muscle contraction sensors) [102,103], to high (> 60%) for high-strain DEAs [104].

This communication presents a method for making compliant electrodes that have a maximum conductivity of ~50 S/cm (corresponding to a sheet resistance[3] of 2 Ω/square) when unstretched and that do not lose conductivity until elongated by over 100%. The electrodes have a secant modulus under 10 MPa, and they show no sign of electrical or mechanical fatigue even after three thousand strain cycles. Upon mechanical relaxation after strain cycling, their conductivity and length recover

[3] Sheet resistance is given by $\frac{1}{\sigma t}$, where σ is the bulk conductivity, and t is the film thickness, which was 0.01 cm.

nearly to their initial values, signifying a low electrical and mechanical hysteresis. The electrodes are photopatternable, making them compatible with microfabrication technology. This enables the fabrication of meso- to micro-scale electrodes for stretchable circuits, retinal implants, or high-deformation microelectromechanical systems (MEMS).

The electrode fabrication method reported here was based on a previously published procedure [30], which had been inspired by ionic polymer-metal composites (IPMCs) [89,90], but in that procedure the reducing solution did not contain methanol, just water as the solvent. Those electrodes only exhibited electrical conductivities of 1 S/cm and strains of 30% before electrical failure [30]. The platinum metal reduced predominantly on the surface of the elastomer, presumably because the metal cations diffused to the surface during reduction, whereas the $NaBH_4$ did not diffuse into the polymer. Under high strain rates (10 %/sec), this metal layer cracked and wrinkled, and the electrodes lost electrical conductivity.

To increase the penetration of the reducing agent into the polymer, we aimed to open the polymer matrix by swelling it in a solvent. Increasing the matrix porosity would be expected to both quicken the reaction and augment the platinum metal penetration depth, thus rendering the polymer-metal adhesion more robust. A faster reaction would also reduce the amount of Pt salt diffusing into the solution, resulting in a higher metal content in the film. Simultaneously, swelling would serve to mechanically strain the polymer during metal build-up, and as the polymer relaxed

after removal from the reduction solution, the metal would fold into out-of-plane corrugations. Corrugations straighten out under strain, allowing metal-coated elastomers to undergo large mechanical elongations before the metal film breaks [18].

The electrodes were fabricated by mixing a Pt salt (tetraammineplatinum(II) chloride) into a liquid elastomer precursor (Loctite 3108, Henkel, Inc.) and then curing the mixture under ultraviolet light (365 nm) for less than a minute. To create the samples for the measurements presented here, the mixture was blanket-exposed and then cut into rectangular strips. However, to pattern the films, the mixture can be exposed through a photomask and developed in ethyl acetate or acetone [29]. We have previously shown that photo-patterning yields a feature resolution of 35 μm in 3108 films 30 μm thick [29], and the addition of the Pt salt does not significantly change the exposure times. The films were rendered conductive by immersing the elastomer in a 30 mM sodium borohydride reducing solution containing 50% water and 50% methanol by volume for an hour. Methanol was used because it is fully miscible in water and swells the Loctite 3108 elastomer by 55%, whereas water only swells it 10% [29]. (Methanol could not be used alone for the solvent: water was needed to dissolve the platinum salt and enable the reaction[4].) As predicted, the reduction proceeded more quickly than in 100% water, taking only one hour instead of ten.

[4] 100% methanol could not be used because the Pt salt is insoluble in methanol. Reduction occurs when $Pt(NH_3)_4 \cdot Cl_2$ dissociates into $[Pt(NH_3)_4]^{2+}$ and Cl^-, which react with $NaBH_4$ and hydroxyl ions to form Pt and by-products [98].

The scanning electron micrographs (SEMs) in Figure 23 show a 3108/Pt film produced using this method with 11 vol.% Pt salt added to the precursor. The surface image in Figure 23a shows that interconnected platinum nodules accumulated on the surface and folded into out-of-plane wrinkles, induced by removal of the *in situ* swelling strain present during metal reduction. The platinum penetrated the 3108 matrix to a depth of ca. 700 nm, as shown in the cross-sections in Figure 23b-c. The brightness of the platinum in the SEM image decreases from the surface to the interior of the polymer, identifying the presence of a platinum concentration gradient. This is confirmed by the transmission electron microscopy (TEM) image, which shows that dispersed platinum nodules are present even several μm below the Pt skin on the surface, suggesting that the metal should adhere well to the polymer. This cross-sectional platinum distribution is similar to that in IPMCs; however, the penetration depth in IPMCs is greater (up to 20 μm) due to repeated reduction steps [89].

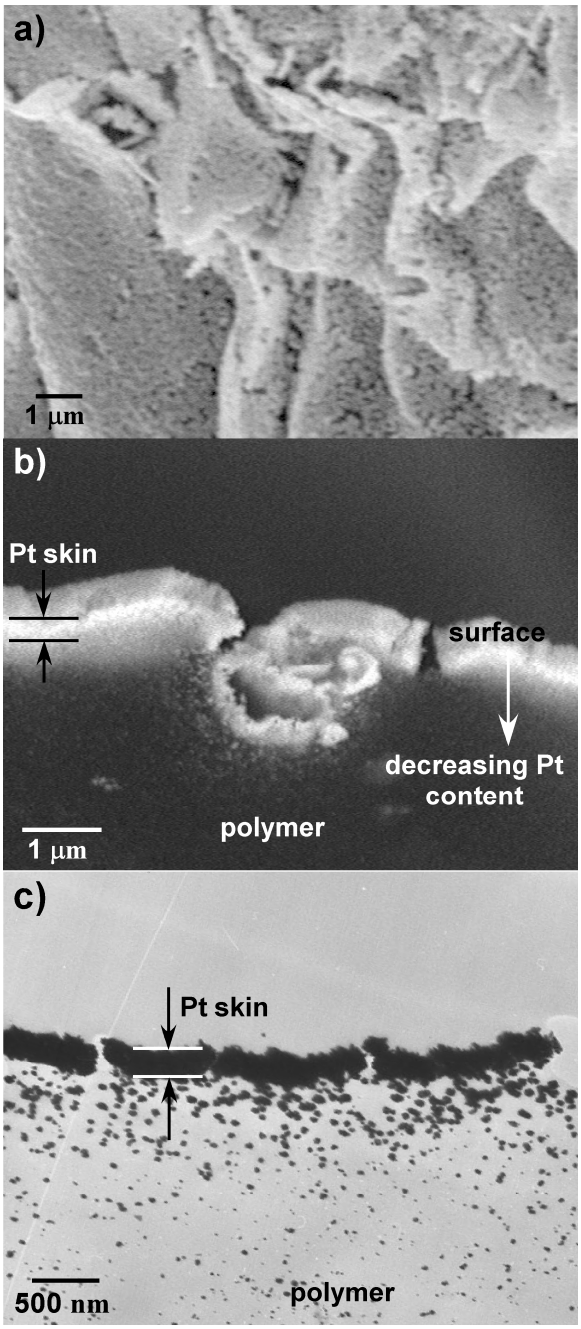

Figure 23. SEMs of the a) surface (15 kV) and b) cross-section (20 kV and back-scattered electron detector) of an 11 vol.% 3108/Pt composite. In b), the sample was microtomed and tilted slightly, so that the top surface is visible above the cross-section. c) TEM of the cross-section of this composite.

High electrical conductivity is advantageous to avoid power dissipation and resistive heating. The resistance of the 3108/Pt composites was measured using a two-point-probe technique. The conductivity was calculated based on the entire film thickness, length, and width and is thus a conservative number: thinner films of the elastomer would yield higher conductivity values. In Figure 24 the conductivity is plotted versus Pt salt concentration in the precursor to determine the percolation threshold[5], which was between 6 and 7%. These results are compared with those from samples reduced in 100% water [30]. The percolation threshold of the methanol samples was sharper, and the conductivity increased beyond that of the water-only samples (0.6 S/cm) to a maximum of 46 S/cm at 15 vol.%. Furthermore, the conductivity continued to increase even above 10 vol.%, while the conductivity in the water samples reached a maximum at 9%. Figure 24 suggests that increasing the salt concentration above 15 vol.% may increase the conductivity even further.

[5] The amount of metal in the final film is a) non-uniform and b) unknown, so salt loading was used as a surrogate parameter.

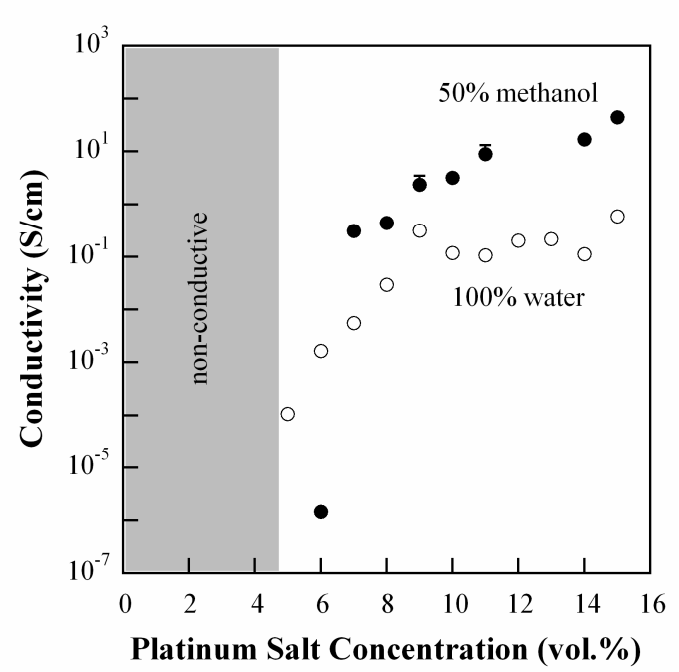

Figure 24. Comparison of the electrical conductivities vs. salt loading of 3108/Pt compliant electrodes reduced in 100% water and in 50/50 water and methanol. Error bars, based on at least three samples each, are plotted for 9-14 vol.% samples; they are too small to be seen on the 10 and 14 vol.% data points.

For compliant electrode applications such as dielectric elastomer actuators, high mechanical strain without electrical failure is critical. To test the maximum strain of the 3108/Pt composites, we monitored the electrical resistance while straining the films at a rate of 0.2 %/second[6]. The maximum strain was defined as the point at which the electrical resistance reached 10^4 times its initial value[7]. The strain to electrical failure tests are summarized in Figure 25a for 9 and 11 vol.% composites. For the 9 vol.% samples, the average achievable strain before failure was 73 +/- 9%,

[6] A low strain rate was chosen to minimize viscoelastic effects [30].
[7] This is not to be confused with the mechanical yield limit of the material.

and for the 11 vol.% samples it was substantially higher at 116 +/- 20%. This is not unexpected because the higher loading means that the film can be stretched more before the areal density of Pt nodules drops below the percolation threshold. The strains for the 11 vol.% electrodes were somewhat higher than those reported for out-of-plane gold corrugations on PDMS membranes [18]. The strain in two 14 vol.% samples (145%) was even higher. Moreover, the electrical conductivity was recoverable, even after straining beyond electrical failure. (Samples produced with water only did not recover after straining to electrical failure.) The conductivity of the 9 vol.% samples, for example, recovered to 50% of the original values following electrical failure testing.

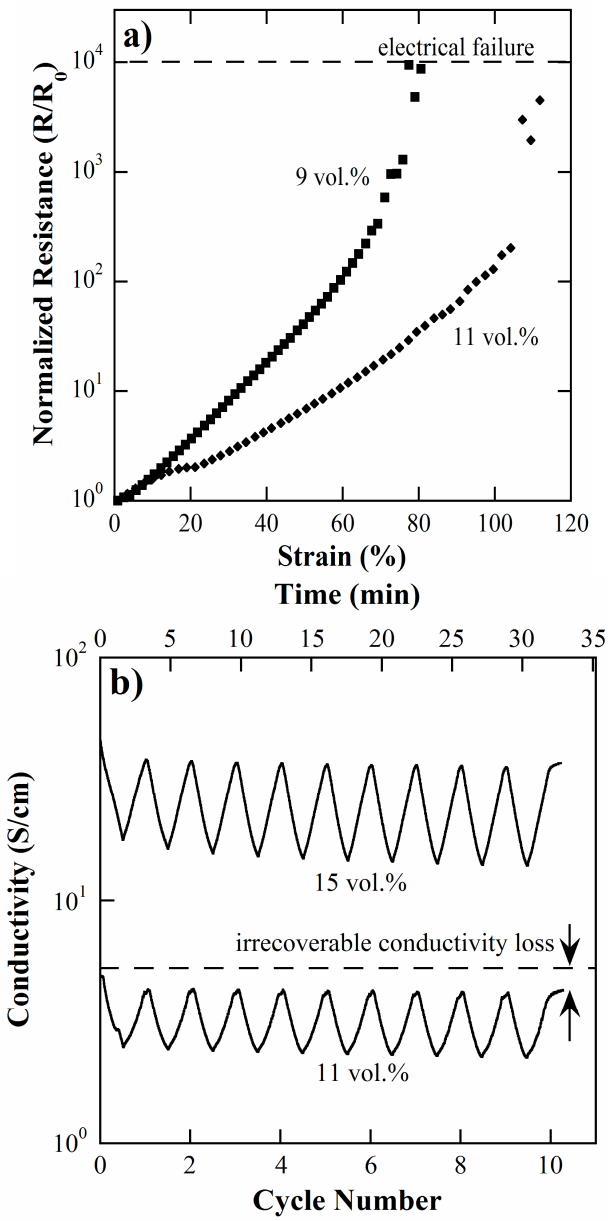

Figure 25. a) Strain to electrical failure for 9 and 11 vol.% 3108/Pt samples. b) Strain cycling from 0 to 20% elongation at a rate of 0.2 % per second for 11 and 15 vol.% loaded 3108/Pt samples.

While these electrodes can withstand high mechanical strain before electrical failure, they should also be able to undergo strain cycling with reproducible behavior and

little hysteresis. Hysteresis may not affect the performance of slow-moving or short-lifetime actuators, but it is critical for other transducers: electrical hysteresis would lead to poor resolution in sensing applications such as strain gauges, for example. Similarly, mechanical hysteresis can adversely affect devices such as DEAs, not only by decreasing lifetime but also by compromising achievable bandwidth, and it can be detrimental for positioning or switching applications. Figure 25b shows 10 strain cycles between 0 and 20% elongation at a strain rate of 0.2 %/second for 11 and 15 vol.% samples.

For both sets of samples (three samples each), the conductivity was linear with strain during both elongation and contraction, and no mechanical hysteresis was observed. (The latter had been a problem in samples reduced in water only [30].) These characteristics are attractive for applications such as strain gauges and pulse monitors, which require a repeatable, linear resistance response to strain. There was, however, some irrecoverable conductivity loss during the first strain cycle. For the 11 vol.% 3108/Pt film shown in Figure 25b, the conductivity began at 5.0 S/cm and decreased to 2.3 S/cm during the 10 cycles; the conductivity subsequently recovered to 4.3 S/cm 45 seconds after testing, a loss of 14% (the average for all samples was 20 +/- 8%). In the 15 vol.% sample in Figure 25b, the behavior was similar, with a conductivity loss of 20% (the average for all samples was 23 +/- 6%).

While the results in Figure 25b are promising, the strain rate with which the films were cycled was quite low, especially for robotic applications. Therefore, we

subjected the composites to lifetime tests at the higher strain rate of 1 Hz (10-60 %/second strain rate): sequential 1000-cycle segments from 0 to 5, 10 (not shown), and 20% strain. The results are shown in Figure 26a. The plotted lines are smoothed curves that show the average peak-to-peak resistance during each cycle. Both the 10 and 11 vol.% samples survived the first 3000 cycles to 5, 10, and 20% strain. In all cases, the average resistance increased during the first several hundred cycles, but then it reached a steady-state value. Although the 11 vol.% samples had a higher initial conductivity, their resistance increase was more pronounced during cycling. For example, the average resistance during the lifetime tests to 20% strain (Figure 26a) stabilized at 55 times the initial value, compared to 16 times for the 10 vol.% sample. One minute after completion of the first 3000 cycles, the resistances recovered to 1.3 and 1.4 times the initial value for 10 and 11 vol.% samples, respectively. The water-only samples had failed at these strain rates [30], whereas these maintained electrical conductivity. This, combined with the fact that these films recover conductivity after being strained beyond electrical failure, indicates that adhesion at the polymer/metal interface was enhanced by the deeper Pt penetration within the elastomer, minimizing conductivity losses and preventing metal delamination.

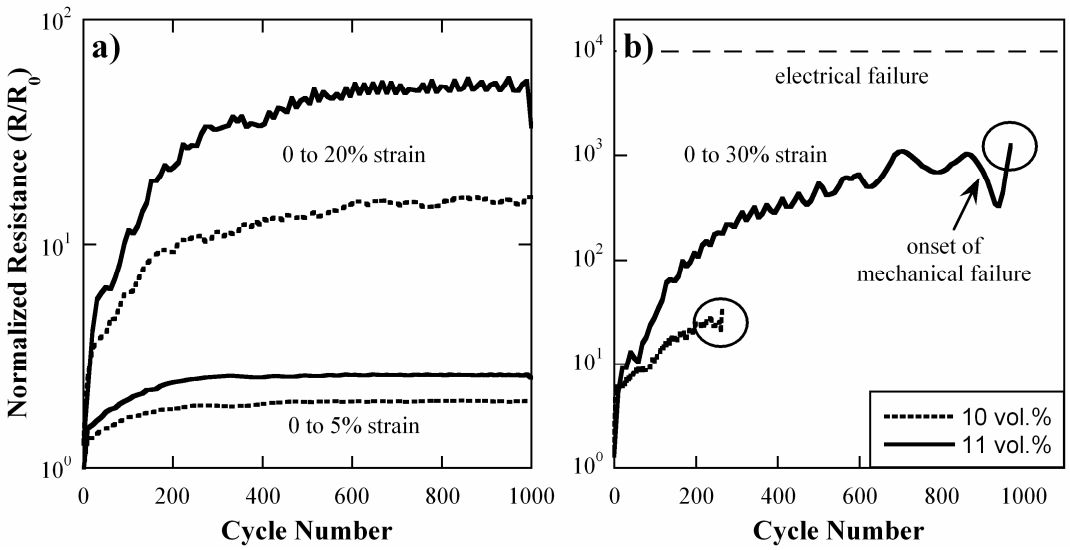

Figure 26. a) 1000-cycle lifetime tests to 5% and 20%, and b) 30% strain at a frequency of 1 Hz for films made with 10 and 11 vol.% salt. The circled regions denote the time at which the samples broke.

The compliant electrodes were then cycled to 30% strain (Figure 26b). However, both 10 and 11 vol.% samples failed mechanically during this test, tearing along the film width. Results based on two samples each of 10 and 11 vol.% electrodes suggested that the 10 vol.% samples fail hundreds of cycles before the 11 vol.% ones (250 and 400 cycles to 30% strain compared to 975 and 990, respectively). Unloaded 3108, on the other hand, survived all 4000 cycles, including the 1000 cycles from 0 to 30% strain, suggesting that the platinum salt decreased the fatigue resistance of the 3108 matrix. Additional optimization of the fabrication process is needed to improve the durability of the electrodes.

The fabrication process for the 3108/Pt composite material presented here has several advantages over the one reported previously [30]. An electrical conductivity between 10^1 and 10^2 S/cm, a maximum strain before failure nearing 150%, and conductivity loss of only 30% after thousands of cycles at high strain rates expand the number of applications for which these compliant electrodes can be used. The lifetime results are promising for pulse monitors, which would require strains of up to 60% at frequencies from 1-3 Hz [103]. The conductivity and achievable strain can easily be tuned to suit a particular purpose by changing the metal salt concentration. Also of note, since the compliant electrodes failed mechanically but not electrically during lifetime testing, it seems that the elastomer matrix was not reinforced by the loaded particles, as one might assume, but weakened by voids created from Pt salt diffusing to the elastomer surface during the reduction reaction. Although these composites in their present form are suitable for many applications, further research on their bandwidth and lifetime is needed before they can be used as electrodes for DEAs, which operate in the kHz frequency range for millions of cycles.

Experimental

Samples were prepared according to [30], except that the reduction solution consisted of 250 mL of methanol, 250 mL of deionized water, and 500 mg of sodium borohydride ($NaBH_4$).

Scanning electron micrographs were taken on an AMRAY 1820D at 15-20 kV. Samples for cross-sectional images were encased in Spurr's resin epoxy (prepared

with 24 wt.% vinyl cyclohexene dioxide, 15 wt.% diglycidyl ether of polypropylene glycol, 61 wt.% nonenyl succinic anhydride, and 0.0004 wt. % dimethylaminoethanol) and sectioned to a thickness of 50-100 nm using a Leica EM UC6 microtome. Transmission electron microscopy (TEM) was performed on a Hitachi H-600.

Conductivity was measured using a two-point probe method (previously described [30]) on 40 mm * 3 mm * 100 μm samples contacted at either end by aluminum clamps. Strain cycling and strain to failure measurements were also performed according to [30].

References

[1] J. M. Engel, N. Chen, K. Ryu, S. Pandya, C. Tucker, Y. Yang, and C. Liu, "Multi-layer embedment of conductive and non-conductive PDMS for all-elastomer MEMS," Solid State Sensors, Actuators, and Microsystems Workshop, Hilton Head, SC, **in press,** p. 316-319 (June 4-8, 2006).

[2] M. Fihn, "The challenges of commercializing flexible displays," *Solid State Technol.*, **49** (5)**,** 43+ (2006).

[3] P. Tsotra and K. Friedrich, "Electrical and mechanical properties characterization of epoxy resin/polyaniline-dodecylbenzenesulphonic acid salt composite materials," *J. Polym. Mat.*, **19,** 389-394 (2002).

[4] L. Johnson, F. K. Perkins, T. O'Hearn, P. Skeath, C. Merritt, J. Frieble, S. Sadda, M. Humayun, and D. Scribner, "Electrical stimulation of isolated retina with microwire glass electrodes," *J. Neurosci. Meth.*, **137** (2)**,** 265-273 (2004).

[5] R. F. Service, "Electronic textiles charge ahead," *Science*, **301** (5635)**,** 909-911 (2003).

[6] S. P. Lacour, C. Tsay, and S. Wagner, "An elastically stretchable TFT circuit," *IEEE Electr. Device L.*, **25** (12)**,** 792-794 (2004).

[7] R. Pelrine, R. Kornbluh, J. Joseph, and S. Chiba, "Electrostriction of polymer films for microactuators," MEMS97, Nagoya, Japan, (IEEE & ASME), p. 238 (Jan. 26-30, 1998).

[8] K. Pope, A. Tews, M. I. Frecker, E. Mockenstrum, N. Goulbourne, and A. J. Snyder, "Dielectric elastomer laminates for active membrane pump applications," Proc. SPIE's 11th Int. Symp. Smart Struc. Mater., Electroactive Polymer Actuators and Devices (EAPAD), San Diego, CA, **vol. 5385**, p. 60-67 (14-18 March, 2004).

[9] Q. Pei, M. Rosenthal, S. Stanford, H. Prahlad, and R. Pelrine, "Multiple-degrees-of-freedom electroelastomer roll actuators," *Smart Mater. Struct.*, **13** (5)**,** N86-N92 (2004).

[10] R. Heydt, R. Kornbluh, R. Pelrine, and V. Mason, "Design and performance of an electrostrictive-polymer-film acoustic actuator," *J. Sound Vib.*, **215** (2)**,** 297-311 (1998).

[11] R. Heydt, R. Pelrine, J. Joseph, J. Eckerle, and R. Kornbluh, "Acoustical performance of an electrostrictive polymer film loudspeaker," *J. Acoust. Soc. Am.*, **107** (2)**,** 833-839 (2000).

[12] S. P. Lacour, H. Prahlad, R. Pelrine, and S. Wagner, "Mechatronic system of dielectric elastomer actuators addressed by thin film photoconductors on plastic," *Sens. Act. A*, **111** (2-3)**,** 288-292 (2004).

[13] S. Zeng, C.-H. Chen, J. C. Mikkelsen, and J. G. Santiago, "Fabrication and characterization of electroosmotic micropumps," *Sens. Act. B*, **79** (2-3)**,** 107-114 (2001).

[14] D. S. Reichmuth, G. S. Chirica, and B. J. Kirby, "Increasing the performance of high-pressure, high-efficiency electrokinetic micropumps using zwitterionic solute additives," *Sens. Act. B*, **92** (1-2)**,** 37-43 (2003).

[15] Y. Takamura, H. Onoda, H. Inokuchi, S. Adachi, A. Oki, and Y. Horiike, "Low-voltage electroosmosis pump for stand-alone microfluidics devices," *Electrophoresis*, **24** (1-2)**,** 185-192 (2003).

[16] R. Pelrine, R. Kornbluh, J. Joseph, R. Heydt, Q. B. Pei, and S. Chiba, "High-field deformation of elastomeric dielectrics for actuators," *Mat. Sci. Eng. C*, **11** (2)**,** 89-100 (2000).

[17] D. S. Gray, J. Tien, and C. S. Chen, "High-conductivity elastomeric electronics," *Adv. Mater.*, **16** (5)**,** 393-397 (2004).

[18] S. P. Lacour, S. Wagner, Z. Y. Huang, and Z. Suo, "Stretchable gold conductors on elastomeric substrates," *Appl. Phys. Lett.*, **82** (15)**,** 2404-2406 (2003).

[19] T. Li, Z. Y. Huang, Z. Suo, S. P. Lacour, and S. Wagner, "Stretchability of thin metal films on elastomer substrates," *Appl. Phys. Lett.*, **85** (16)**,** 3435-3437 (2004).

[20] T. Li, Z. Y. Huang, Z. C. Xi, S. P. Lacour, S. Wagner, and Z. Suo, "Delocalizing strain in a thin metal film on a polymer substrate," *Mech. Mater.*, **37** (2-3)**,** 261-273 (2005).

[21] G. Kofod, P. Sommer-Larsen, R. Kornbluh, and R. Pelrine, "Actuation response of polyacrylate dielectric elastomers," *J. Intel. Mat. Syst. Str.*, **14** (12)**,** 787-793 (2003).

[22] F. Gubbels, R. Jerome, P. Teyssie, E. Vanlathem, R. Deltour, A. Calderone, V. Parente, and J. L. Bredas, "Selective localization of carbon black in

immiscible polymer blends: a useful tool to design electrical conductive composites," *Macromolecules*, **27** (7)**,** 1972-1974 (1994).

[23] S. Jiguet, A. Bertsch, H. Hofmann, and P. Renaud, "Conductive SU8 photoresist for microfabrication," *Adv. Funct. Mater.*, **15,** 1511-1516 (2005).

[24] R. Faez, W. A. Gazotti, and M.-A. De Paoli, "An elastomeric conductor based on polyaniline prepared by mechanical mixing," *Polymer*, **40,** 5497-5503 (1999).

[25] K. P. Sau, T. K. Chaki, and D. Khastgir, "Carbon fibre filled conductive composites based on nitrile rubber (NBR), ethylene propylene diene rubber (EPDM) and their blend," *Polymer*, **39** (25)**,** 6461-6471 (1998).

[26] R. Delille, M. Urdaneta, K. Hsieh, and E. Smela, "Novel compliant electrodes based on platinum salt reduction," Proc. SPIE's 13th Int. Symp. Smart Struc. Mater., Electroactive Polymer Actuators and Devices (EAPAD), San Diego, CA, **vol. 6168** (26 Feb - 2 Mar, 2006).

[27] W. Lu, E. Smela, P. Adams, G. Zuccarello, and B. R. Mattes, "Development of solid-in-hollow electrochemical linear actuators using highly conductive polyaniline," *Chem. Mater.*, **16** (9)**,** 1615-1621 (2004).

[28] Nanosonic, "Material Properties Sheet, Metal Rubber", 2006.

[29] R. Delille, M. Urdaneta, S. Moseley, and E. Smela, "Benchtop Polymer MEMS," *J. Microelectromech. S.*, **in press** (2006).

[30] R. Delille, M. Urdaneta, K. Hsieh, and E. Smela, "Compliant electrodes based on platinum salt reduction in a urethane matrix," *Smart Mater. Struct.*, **in press** (2006).

[31] R. Delille, M. Urdaneta, and E. Smela, "High-Strain, High-Conductivity Photopatternable Electrodes," *Adv. Mater.*, **submitted** (2006).

[32] E. Kim, Y. Xia, and G. M. Whitesides, "Polymer microstructures formed by moulding in capillaries," *Nature*, **376** (6541)**,** 581-584 (1995).

[33] Y. Xia, M. Mrksich, E. Kim, and G. M. Whitesides, "Microcontact printing of octadecylsiloxane on the surface of silicon dioxide and its application in microfabrication," *J. Am. Chem. Soc.*, **117** (37)**,** 9576-9577 (1995).

[34] D. J. Beebe, J. S. Moore, Q. Yu, R. H. Liu, M. L. Kraft, B.-H. Jo, and C. Devadoss, "Microfluidic tectonics: A comprehensive construction platform for microfluidic systems," *PNAS*, **97** (25)**,** 13488–13493 (2000).

[35] W. R. Childs and R. G. Nuzzo, "Decal transfer microlithography: a new soft-lithographic patterning method," *J. Am. Chem. Soc.*, **124,** 13583-13596 (2002).

[36] M. Aguirregabiria, F. J. Blanco, J. Berganzo, J. Ruano, I. Aranburu, J. Garcia, and K. Mayora, "Novel SU8 multilayer technology based on succesive CMOS compatible adhesive bonding and Kapton releasing steps for multilevel microfluidic devices," MicroTAS 2004, Malmö, Sweden, **vol. 2**, p. 49-51 (Sept. 26-30, 2004).

[37] J. Ruano, M. Aguirregabiria, M. T. Arroyo, J. Berganzo, F. J. Blanco, P. de la Fuente, E. Castano, and K. Mayora, "An optical microfluidic platform based on a combination of a novel SU8 multilayer technology, waveguides and photodiodes on silicon," MicroTAS 2004, Malmö, Sweden, **vol. 2**, p. 34-36 (Sept. 26-30, 2004).

[38] K. Atsuta, H. Suzuki, and S. Takeuchi, "Fine patterning of protein with parylene sheet," MicroTAS 2004, Malmö, Sweden, **vol. 2**, p. 249-251 (Sept. 26-30, 2004).

[39] A. Butterworth, M. del Carmen Lopez Garcia, and D. J. Beebe, "Photopolymerized poly(ethylene) glycol diacrylate (PEGDA) microfluidic devices," MicroTAS 2004, Malmö, Sweden, **vol. 2**, p. 4-6 (Sept. 26-30, 2004).

[40] P. Vulto, N. Glade, L. Altomare, J. Bablet, G. Medoro, A. Leonardi, A. Romani, I. Chartier, N. Manaresi, M. Tartagni, and R. Guerrieri, "Dry film resist for fast fluidic prototyping," MicroTAS 2004, Malmö, Sweden, **vol. 2**, p. 43-45 (Sept. 26-30, 2004).

[41] A. Sudarsan, J. Wang, and V. M. Ugaz, "Novel thermoplastic elastomers for microfluidic device construction," MicroTAS 2004, Malmö, Sweden, **vol. 2**, p. 22-24 (Sept. 26-30, 2004).

[42] W. G. Koh, A. Revzin, and M. V. Pishko, "Poly(ethylene glycol) hydrogel microstructures encapsulating living cells," *Langmuir*, **18** (7)**,** 2459-2462 (2002).

[43] J. C. McDonald and G. M. Whitesides, "Poly(dimethylsiloxane) as a material for fabricating microfluidic devices," *Acc. Chem. Res.*, **35** (7)**,** 491-499 (2002).

[44] M. J. Felton, "CD simplicity: compact disc-based fluidics is an evolving form of lab-on-a-chip technology," *Mod. Drug Disc.* (Nov.)**,** 35-39 (2003).

[45] D. Pede, G. Serra, and D. De Rossi, "Microfabrication of conducting polymer devices by ink-jet stereolithography," *Mat. Sci. Eng. C*, **C5** (3-4)**,** 289-291 (1998).

[46] S. B. Fuller, E. J. Wilhelm, and J. A. Jacobson, "Ink-jet printed nanoparticle microelectromechanical systems," *J. Microelectromech. Syst.*, **11** (1)**,** 54-60 (2002).

[47] D. Daniel and I. G. R. Gutz, "Quick production of gold electrode sets or arrays and of microfluidic flow cells based on heat transfer of laser printed toner masks onto compact discs," *Electrochem. Commun.*, **5** (9)**,** 782-786 (2003).

[48] G. M. Whitesides, "Microfabrication, microfluidics, and biomedicine: new tools and new opportunities," MicroTAS 2005, 9th Intl. Conf. on Miniaturized Systems for Chemistry and Life Sciences, Boston, MA, edited by K. F. Jensen, J. Han, D. J. Harrison, and J. Voldman, p. plenary lecture (Oct. 9-13, 2005).

[49] C. Khoury, G. A. Mensing, and D. J. Beebe, "Ultra rapid prototyping of microfluidic systems using liquid phase photopolymerization," *Lab Chip*, **2** (1)**,** 50-55 (2002).

[50] Loctite, "Product Description Sheet, Product 3108", http://tds.loctite.com/tds5/docs/3108-EN.PDF, 2002.

[51] Loctite, "Technical Data Sheet, Product 3340", http://tds.loctite.com/tds5/docs/3340-EN.PDF, 2002.

[52] Loctite, "Technical Data Sheet, Loctite 3525", http://tds.loctite.com/tds5/docs/3525-EN.PDF, 2004.

[53] D. C. Duffy, J. C. McDonald, O. J. A. Schueller, and G. M. Whitesides, "Rapid prototyping of microfluidic systems in poly(dimethylsiloxane)," *Anal. Chem.*, **70** (23)**,** 4974-4984 (1998).

[54] P. Argyrakis, L. Teo, T. Stevenson, and R. Cheung, "Fabrication of PDMS stamps for the patterned growth of carbon nanotubes," *Microelectron. Eng.*, **78-79,** 647-652 (2005).

[55] J. N. Lee, C. Park, and G. Whitesides, "Solvent compatibility of poly(dimethylsiloxane)-based microfluidic devices," *Anal. Chem.*, **75** (23)**,** 6544-6554 (2003).

[56] J. S. Yoo, S. J. Kim, and J. S. Choi, "Swelling equilibria of mixed solvent/poly(dimethylsiloxane) systems," *J. Chem. Eng. Data*, **44** (1)**,** 16-22 (1999).

[57] Y. Du, Y. Xue, and H. L. Frisch, "Ch. 16, Solubility Parameters," in Physical Properties of Polymers Handbook, Vol. XV of the series AIP Series in Polymers and Complex Materials, edited by J. E. Mark, p. 227-239 (AIP Press, Woodbury, NY, 1996).

[58] P. Abshire, J.-M. Lauenstein, Y. Liu, and E. Smela, "Cell clinics for bioelectronic interface with single cells," IEEE Int. Symp. Circuits and Systems (ISCAS03), Bangkok, Thailand (May 25-28, 2003).

[59] Y. Liu, N. M. Nelson, P. Abshire, and E. Smela, "Biolab-on-a-chip for capturing, culturing, and in-situ investigation of living cells," MicroTAS 2004, Malmö, Sweden, **vol. 2**, p. 584-586 (Sept. 26-30, 2004).

[60] M. Urdaneta, Y. Liu, M. Christophersen, S. Prakash, P. Abshire, and E. Smela, "Integrating conjugated polymer microactuators with CMOS sensing circuitry for studying living cells," SPIE's 12th Annual Int'l. Symp. Smart Structures and Materials, EAPAD, San Diego, CA, edited by Y. Bar-Cohen, p. 232-240 (March 7-10, 2005).

[61] S. B. Prakash, P. Abshire, M. Urdaneta, and E. Smela, "A CMOS capacitance sensor for cell adhesion characterization," Int. Symp. Circuits & Systems (ISCAS05), Kobe, Japan, (IEEE), p. 3495 - 3498 (23-26 May, 2005).

[62] T. Henning, M. Brischwein, W. Baumann, R. Ehret, I. Freund, R. Kammerer, M. Lehmann, A. Schwinde, and B. Wolf, "Approach to a multiparametric sensor-chip-based tumor chemosensitivity assay," *Anti-Cancer Drugs*, **12,** 21 - 32 (2001).

[63] A. Lambacher, M. Jenkner, M. Merz, B. Eversmann, R. A. Kaul, F. Hofmann, R. Thewes, and P. Fromherz, "Electrical imaging of neuronal activity by multi-transistor-array (MTA) recording at 7.8 μm resolution," *Appl. Phys. A*, **79** (7)**,** 1607-1611 (2004).

[64] S. Vassanelli and P. Fromherz, "Neurons from rat brain coupled to transistors," *Appl. Phys. A*, **65,** 85 - 88 (1997).

[65] E. G. Cen, C. Dalton, Y. Li, S. Adamia, L. M. Pilarski, and K. V. I. S. Kaler, "A combined dielectrophoresis, traveling wave dielectrophoresis and electrorotation microchip for the manipulation and characterization of human malignant cells," *J Microbiol. Meth.*, **58** (3)**,** 387 - 401 (2004).

[66] J. Zhang, "LIGA mold insert fabrication using SU-8 photoresist," MS Thesis, Mechanical Engineering, Louisiana State University (2002).

[67] C. Harrison, J. T. Cabral, C. M. Stafford, A. Karim, and E. J. Amis, "A rapid prototyping technique for the fabrication of solvent-resistant structures," *J. Micromech. Microeng.*, **14** (1)**,** 153-158 (2004).

[68] L. Gammelgaard, P. Rasmussen, M. Calleja, and A. Boisen, "SU-8 cantilever strain sensor with integrated readout based on a piezoresistive SU-8/carbon black composite," MicroTAS 2004, Malmö, Sweden, **vol. 2**, p. 482-484 (Sept. 26-30, 2004).

[69] S. Jiguet, A. Bertsch, H. Hofmann, and P. Renaud, "Conductive SU8-silver composite photopolymer," 17th IEEE Int'l. Conf. Micro Electro Mechanical Systems, Maastricht, The Netherlands, p. 125-128 (January 25-29, 2004).

[70] D. Nilsson, S. Balsley, and A. Kristensen, "Solid polymer dye laser based on a single mode SU-8 planar waveguide," MicroTAS 2004, Malmö, Sweden, **vol. 2**, p. 369-371 (Sept. 26-30, 2004).

[71] M. Khoo and C. Liu, "Micro magnetic silicone elastomer membrane actuator," *Sens. Act. A*, **89** (3)**,** 259-266 (2001).

[72] G. T. A. Kovacs, *Micromachined Transducers Sourcebook*, (WCB McGraw-Hill, Boston, 1998).

[73] L. K. Lagorce, O. Brand, and M. G. Allen, "Magnetic microactuators based on polymer magnets," *J. Microelectromech. Syst*, **8** (1)**,** 2-9 (1999).

[74] W. Wang, Z. Yao, J. Chen, and J. Fang, "Composite elastic magnet films with hard magnetic feature," *J. Micromech. Microeng.*, **14** (10)**,** 1321-1327 (2004).

[75] M. Farshad and A. Benine, "Magnetoactive elastomer composites," *Polym. Test.*, **23** (3)**,** 347-353 (2004).

[76] L. K. Lagorce and M. G. Allen, "Magnetic and mechanical properties of micromachined strontium ferrite/polyimide composites," *J. Microelectromech. Syst.*, **6** (4)**,** 307-312 (1997).

[77] D. R. Saini, A. V. Shenoy, and V. M. Nadkarni, "Effect of surface treatments on rheological, mechanical, and magnetic properties of ferrite-filled polymeric systems," *Polym. Eng. Sci.*, **25** (13)**,** 807-811 (1985).

[78] S. R. Shinde, A. Bhagwat, S. I. Patil, S. B. Ogale, G. K. Mehta, S. K. Date, and G. Marest, "Influence of 85 MeV oxygen ion irradiation on magnetization behavior of micron-sized and nano-sized powders of strontium ferrite ($SrFe_{12}O_{19}$)," *J. Magn. Magn. Mater.*, **186,** 342-348 (1998).

[79] Norland Products, "Optical/UV Adhesives", http://www.norlandprod.com/adhesives/adhindex.tpl?category=NOA, 2005.

[80] E. Smela, O. Inganäs, and I. Lundström, "Controlled folding of micrometer-size structures," *Science*, **268** (23 June)**,** 1735-1738 (1995).

[81] W. Ko, "The future of sensor and actuator systems," *Sens. Act. A*, **56** (1-2)**,** 193-197 (1996).

[82] S. Ashley, "Artificial muscles," *Sci. Am.*, **289** (4)**,** 52-59 (2003).

[83] E. Schnack, B. Prinz, and S. Dimitrov, "Interlaminar stress determination in carbon fibre epoxy composites with the embedded strain gauge technique," *Strain*, **40** (3)**,** 113-118 (2004).

[84] R. Pelrine, R. Kornbluh, Q. B. Pei, and J. Joseph, "High-speed electrically actuated elastomers with strain greater than 100%," *Science*, **287** (5454)**,** 836-839 (2000).

[85] M. Watanabe, H. Shirai, and T. Hirai, "Wrinkled polypyrrole electrode for electroactive polymer actuators," *J. Appl. Phys.*, **92** (8)**,** 4631-4637 (2002).

[86] J. Jones, S. P. Lacour, S. Wagner, and Z. G. Suo, "Stretchable wavy metal interconnects," *J. Vac. Sci. Technol. A*, **22** (4)**,** 1723-1725 (2004).

[87] R. E. Pelrine, R. D. Kornbluh, and J. P. Joseph, "Electrostriction of polymer dielectrics with compliant electrodes as a means of actuation," *Sens. Act. A*, **64** (1)**,** 77-85 (1998).

[88] K. Onishi, S. Sewa, K. Asaka, N. Fujiwara, and K. Oguro, "Morphology of electrodes and bending response of the polymer electrolyte actuator," *Electrochim. Acta*, **46** (5)**,** 737-743 (2000).

[89] M. Shahinpoor and K. J. Kim, "Ionic polymer-metal composites: I. Fundamentals," *Smart Mater. Struct.*, **10** (4)**,** 819-833 (2001).

[90] K. J. Kim and M. Shahinpoor, "Ionic polymer-metal composites: II. Manufacturing techniques," *Smart Mater. Struct.*, **12** (1)**,** 65-79 (2003).

[91] S. Nemat-Nasser and Y. X. Wu, "Comparative experimental study of ionic polymer-metal composites with different backbone ionomers and in various cation forms," *J. Appl. Phys.*, **93** (9)**,** 5255-5267 (2003).

[92] K. Yamaguchi, J. J. C. Busfield, and A. G. Thomas, "Electrical and mechanical behavior of filled elastomers. I. The effect of strain," *J. Polym. Sci. Pol. Phys.*, **41** (17)**,** 2079-2089 (2003).

[93] H. Topsoe, "Geometric Factors in Four Point Resistivity Measurement" (1968).

[94] E. Smela and B. R. Mattes, "Polyaniline actuators, part 2: PANI(AMPS) in methanesulfonic acid," *Synthetic Met.*, **151** (1)**,** 43-48 (2005).

[95] Loctite, "Technical Data Sheet, Loctite 4304," (2005).

[96] F. Gubbels, R. Jerome, E. Vanlathem, R. Deltour, S. Blacher, and F. Brouers, "Kinetic and thermodynamic control of the selective localization of carbon black at the interface of immiscible polymer blends," *Chem. Mater.*, **10** (5)**,** 1227-1235 (1998).

[97] M. Shahinpoor and K. J. Kim, "The effect of surface-electrode resistance on the performance of ionic polymer-metal composite (IPMIC) artificial muscles," *Smart Mater. Struct.*, **9** (4)**,** 543-551 (2000).

[98] P. Millet, F. Andolfatto, and R. Durand, "Preparation of solid polymer electrolyte composites - investigation of the precipitation process," *J. Appl. Electrochem.*, **25** (3)**,** 233-239 (1995).

[99] W. D. Callister, *Materials Science and Engineering: An Introduction*, 5th ed. (John Wiley & Sons, New York, 2000).

[100] I. M. Ward and D. W. Hadley, *An Introduction to the Mechanical Properties of Solid Polymers*, (John Wiley & Sons, New York, 1993).

[101] S. P. Lacour, J. Jones, Z. Suo, and S. Wagner, "Design and performance of thin metal film interconnects for skin-like electronic circuits," *IEEE Electr. Device L.*, **25** (4)**,** 179-181 (2004).

[102] C. C. van Donkelaar, P. J. B. Willems, A. M. M. Muijtjens, and M. R. Drost, "Skeletal muscle transverse strain during isometric contraction at different lengths," *J. Biomech.*, **32** (8)**,** 755-762 (1999).

[103] Y. Sharf, Y. Seo, U. Eliav, S. Akselrod, and G. Navons, "Mapping strain exerted on blood vessel walls using deuterium double-quantum-filtered MRI," *Proc. Natl. Acad. Sci. USA*, **95** (8)**,** 4108-4112 (1998).

[104] R. Pelrine, R. Kornbluh, and G. Kofod, "High-strain actuator materials based on dielectric elastomers," *Adv. Mat.*, **12** (16)**,** 1223-1225 (2000).